The new galaxy evolution paradigm revealed by the Herschel surveys

Article (Published Version)

Monthly Notices
of the
ROYAL ASTRONOMICAL SOCIETY

MNRAS **473,** 3507–3524 (2018) doi:10.1093/mnras/stx2548
Advance Access publication 2017 October 12

The new galaxy evolution paradigm revealed by the *Herschel* surveys

Stephen Eales,[1]★ Dan Smith,[2] Nathan Bourne,[3] Jon Loveday,[4] Kate Rowlands,[5,6] Paul van der Werf,[7] Simon Driver,[8] Loretta Dunne,[1,3] Simon Dye,[9] Cristina Furlanetto,[9,10] R. J. Ivison,[3,11] Steve Maddox,[1,3] Aaron Robotham,[8] Matthew W. L. Smith,[1] Edward N. Taylor,[12] Elisabetta Valiante,[1] Angus Wright,[8,13] Philip Cigan,[1] Gianfranco De Zotti,[14,15] Matt J. Jarvis,[16,17] Lucia Marchetti,[18] Michał J. Michałowski,[3,19] Steven Phillipps,[20] Sebastien Viaene[21] and Catherine Vlahakis[22]

[1]*School of Physics and Astronomy, Cardiff University, The Parade, Cardiff CF24 3AA, UK*
[2]*Centre for Astrophysics Research, School of Physics, Astronomy and Mathematics, University of Hertfordshire, College Lane, Hatfield, AL10 9AB, UK*
[3]*Institute for Astronomy, The University of Edinburgh, Royal Observatory, Blackford Hill, Edinburgh, EH9 3HJ, UK*
[4]*Astronomy Centre, University of Sussex, Falmer, Brighton BN1 9QH, UK*
[5]*Scottish Universities Physics Alliance, School of Physics and Astronomy, University of St. Andrews, North Haugh*
[6]*Department of Physics and Astronomy, Johns Hopkins University, Bloomberg Center, 3400 N. Charles St., Baltimore, MD 21218, USA*
[7]*Leiden Observatory, P.O. Box 9513, 2300 RA, Leiden, the Netherlands*
[8]*International Centre for Radio Astronomy Research, 7 Fairway, The University of Western Australia, Crawley, Perth, WA 6009, Australia*
[9]*School of Physics and Astronomy, University of Nottingham, University Park, Nottingham NG7 2RD, UK*
[10]*Departamento de Física, Universidade Federal do Rio Grande do Sul, Av. Bento Gonçalves, 9500, 91501-970 Porto Alegre, RS, Brazil*
[11]*European Southern Observatory, Karl-Schwarzschild-Strasse 2, 85748, Garching, Germany*
[12]*Centre for Astrophysics and Supercomputing, Swinburne University of Technology, Hawthorn 3122, Australia*
[13]*Argelander-Institut fur Astronomie, Auf dem Hugel 71, D-53121 Bonn, Germany*
[14]*INAF-Osservatorio Astronomico di Padova, Vicolo Osservatorio 5, I-35122 Padova, Italy*
[15]*SISSA, Via Bonomea 265, I-34136 Trieste, Italy*
[16]*Astrophysics, Department of Physics, Keble Road, Oxford, OX1 3RH, UK*
[17]*Physics and Astronomy Department, University of the Western Cape, Bellville 7535, South Africa*
[18]*Department of Physical Sciences, The Open University, Milton Keynes, MK7 6AA, UK*
[19]*Astronomical Observatory Institute, Faculty of Physics, Adam Mickiewicz University, ul. Stoneczna 36, 60-286 Poznan, Poland*
[20]*Astrophysics Group, Department of Physics, University of Bristol, Tyndall Avenue, Bristol BS8 1TL, UK*
[21]*Sterrenkundig Observatorium,Universiteit Gent, Krijgslaan 281 S9, B-9000 Gent, Belgium*
[22]*North American ALMA Science Center, National Radio Astronomy Observatory, 520 Edgemont Road, Charlottesville, VA 22901, USA*

Accepted 2017 September 28. Received 2017 September 28; in original form 2016 November 7

ABSTRACT

The *Herschel Space Observatory* has revealed a very different galaxyscape from that shown by optical surveys which presents a challenge for galaxy-evolution models. The *Herschel* surveys reveal (1) that there was rapid galaxy evolution in the very recent past and (2) that galaxies lie on a single Galaxy Sequence (GS) rather than a star-forming 'main sequence' and a separate region of 'passive' or 'red-and-dead' galaxies. The form of the GS is now clearer because far-infrared surveys such as the Herschel ATLAS pick up a population of optically red star-forming galaxies that would have been classified as passive using most optical criteria. The space-density of this population is at least as high as the traditional star-forming population. By stacking spectra of H-ATLAS galaxies over the redshift range $0.001 < z < 0.4$, we show that the galaxies responsible for the rapid low-redshift evolution have high stellar masses, high star-formation rates but, even several billion years in the past, old stellar populations – they are thus likely to be relatively recent ancestors of early-type galaxies in the Universe today. The form of the GS is inconsistent with rapid quenching models and neither the analytic bathtub model nor the hydrodynamical EAGLE simulation can reproduce the rapid cosmic evolution. We propose a new gentler model of galaxy evolution that can explain the new *Herschel* results and other key properties of the galaxy population.

Key words: galaxies: evolution.

★ E-mail: sae@astro.cf.ac.uk

1 INTRODUCTION

Over the last decade a simple phenomenological model of galaxy evolution has been widely used by astronomers to interpret observations. In this model, star-forming galaxies lie on the 'Galaxy Main Sequence' (henceforth GMS), a distinct region in a plot of star-formation rate versus galaxy stellar mass (e.g. Daddi et al. 2007; Elbaz et al. 2007; Noeske et al. 2007; Peng et al. 2010; Rodighiero et al. 2011; Whitaker et al. 2012; Lee et al. 2015). Over cosmic time, the GMS gradually moves downwards in star-formation rate, which decreases by a factor of $\simeq$20 from a redshift of 2 to the current epoch (Daddi et al. 2007). Observations of the molecular gas and dust in galaxies show that the principal cause of this evolution is that high-redshift galaxies contained more gas and therefore formed stars at a faster rate (Tacconi et al. 2010; Dunne et al. 2011; Genzel et al. 2015; Scoville et al. 2016).

In this phenomenological paradigm, an individual galaxy moves along the GMS until some process quenches the star formation in the galaxy, which then moves rapidly (in cosmic terms) across the diagram to the region occupied by 'red and dead' or 'passive' galaxies. Possible quenching processes include galaxy merging (Toomre 1977), with a starburst triggered by the merger rapidly using up the available gas; the expulsion of gas by a wind from an active galactic nucleus (Cicone et al. 2014); the rapid motion of star-forming clumps towards the centre of the galaxy (Noguchi 1999; Bournaud, Elmgreen & Elmgreen 2007; Genzel et al. 2011, 2014), leading to the formation of a stellar bulge, which then stabilizes the star-forming gas disc and reduces the rate at which the gas collapses to form stars (Martig et al. 2009); and a variety of environmental processes which either reduce the rate at which gas is supplied to a galaxy or drive out most of the existing gas (Boselli & Gavazzi 2006).

As can be seen from the long list of possible quenching mechanisms, the physics underlying this paradigm is unknown. Peng et al. (2010) have shown that many statistical properties of star-forming and passive galaxies can be explained by a model in which both the star-formation rate and the probability of quenching are proportional to the galaxy's stellar mass, but the physics behind both proportionalities is unknown. Although it is clear that the increased star-formation rates in high-redshift galaxies are largely due to their increased gas content, there is also evidence that the star-formation efficiency is increasing with redshift (Rowlands et al. 2014; Santini et al. 2014; Genzel et al. 2015; Scoville et al. 2016); so either the physics of star formation or the properties of the interstellar gas (Papadopoulos & Geach 2012) must also be changing with redshift in some way.

Implicit in this paradigm is the assumption that there are two physically distinct classes of galaxy. These two classes of galaxy are variously called 'star-forming' and 'passive', 'star-forming' and 'red-and-dead' or 'star-forming' and 'quenched'. The most visually striking evidence that there are two separate classes is that on plots of optical colour versus optical absolute magnitude, galaxies fall in two distinct areas: a 'blue cloud' of star-forming galaxies and a tight 'red sequence' representing the passive galaxies (e.g. Bell et al. 2004). However, in an earlier paper (Eales et al. 2017), we argued that the tight red sequence is the result of optical colour depending only very weakly on specific star-formation rate (star-formation rate divided by galaxy stellar mass, henceforth SSFR) for SSFR $< 5 \times 10^{-12}$ yr^{-1}; the red sequence is therefore better thought of as the accumulated number of galaxies that have passed below this critical SSFR, all of which pile up at the same colour, rather than representing a distinct class of galaxy. The two classes are largely the same as the morphological classes of early-type and late-type galaxies (henceforth ETGs and LTGs). Although there is plenty of evidence for a gradual change in the properties of galaxies along the morphological Hubble sequence (e.g. Kennicutt 1998), there is now little evidence for a clear dichotomy between the two broad morphological classes (see Section 5.5 of this paper).

The launch in 2009 of the *Herschel Space Observatory* (Pilbratt et al. 2010) gave a different view of the galaxy population from the one given by optical surveys. Apart from the interest of this new galaxyscape, produced by the different selection effects operating on optical and far-infrared surveys (Section 2), *Herschel's* launch provided two immediate practical benefits for astronomers studying galaxy evolution. The first was that *Herschel* made it possible for astronomers to measure directly the part of the energy output of stars that is hidden by dust. For example, by using *Herschel* and other telescopes to measure the bolometric luminosity of different galaxy classes, it is possible to measure the size of the morphological transformation that has occurred in the galaxy population in the last eight billion years (Eales et al. 2015). The second benefit is that with *Herschel* submillimetre photometry, which now exists for $\sim 10^6$ galaxies, it is possible to estimate the mass of a galaxy's ISM from its dust emission (Eales et al. 2012; Scoville et al. 2014; Groves et al. 2015), a technique that has since been profitably extended to ALMA observations (Scoville et al. 2016).

In this paper, we investigate this new galaxyscape. The paper is based on two *Herschel* surveys: the *Herschel* Reference Survey (henceforth HRS) and the *Herschel* Astrophysical Terrahertz Large Area Survey (henceforth H-ATLAS). We describe these surveys in more detail in Section 2 but, briefly, the HRS is a volume-limited sample of 323 galaxies, designed before launch to be a complete as possible census of the stellar mass in the Universe today; each galaxy was then individually observed with *Herschel* (Boselli et al. 2010; Ciesla et al. 2012; Cortese et al. 2012; Smith et al. 2012b; Eales et al. 2017). The H-ATLAS was the largest (in sky area, 660 square degrees) *Herschel* extragalactic survey, consisting of imaging at 100, 160, 250, 350 and 500 μm of five fields, two large fields at the North and South Galactic Poles and three smaller fields on the celestial equator (Eales et al. 2010).

There is already one important advance in our knowledge of galaxy evolution provided by the *Herschel* surveys, although we suspect this has not yet been absorbed by the wider astronomical community. In an early H-ATLAS paper (Dye et al. 2010), we showed that the 250-μm luminosity function evolves remarkably rapidly, even showing significant evolution by a redshift of 0.1, which we have confirmed recently with a much larger dataset (Wang et al. 2016a). We have also shown (Dunne et al. 2011; Bourne et al. 2012) that there is rapid evolution in the masses of dust in galaxies, and therefore in the mass of the ISM. Using radio continuum emission to trace the star formation, we found that there is also rapid evolution at low redshift in the star-formation rates of galaxies (Hardcastle et al. 2016). Marchetti et al. (2016) reached the same conclusion from a different *Herschel* survey and using a different method of estimating the star-formation rate (from the bolometric dust luminosity). This rapid low-redshift evolution is important because, as we show in this paper, it is not predicted by important galaxy-evolution models.

A note on nomenclature: in this paper, we generally use the term 'Galaxy Sequence' rather than 'Galaxy Main Sequence'. The latter term is implicitly based on the phenomenological paradigm, in which galaxies, like stars, spend most of their life in an active phase, which then comes to a definite end. We prefer the empirical term 'Galaxy Sequence', which is free of theoretical assumptions.

Our definition of the term is that it refers to the distribution of galaxies in a plot of specific star-formation rate versus stellar mass that contains most of the stellar mass in a given volume of space.

The arrangement of this paper is as follows. In Section 2, we describe the two *Herschel* surveys in more detail. Sections 3 and 4 describe results from the two surveys that have implications for galaxy evolution. In Section 5, we discuss the implications of these results for the phenomenological paradigm and propose an alternative model for galaxy evolution that is in better agreement with these results. We suggest that readers not interested in the details of the *Herschel* results but interested in their implications skip to Section 5, which we start with a summary of the main observational results. A summary of the main results of this paper is given in Section 6.

We assume a Hubble constant of 67.3 km s^{-1} Mpc^{-1} and the other *Planck* cosmological parameters (Planck Collaboration 2014).

2 THE *Herschel* SURVEYS

The HRS consists of 323 galaxies with distances between 15 and 25 Mpc and with a near-infrared K-band limit of $K < 8.7$ for early-type galaxies (ETGs) and $K < 12$ for late-type galaxies (LTGs; Boselli et al. 2010). The sample was designed to be a volume-limited sample of galaxies selected on the basis of stellar mass. Eales et al. (2017) estimate that within the HRS volume the survey is complete for LTGs with stellar masses above $\simeq 8 \times 10^8$ M$_\odot$ and for ETGs with stellar masses above $\simeq 2 \times 10^{10}$ M$_\odot$. The survey therefore misses low-mass ETGs, but Eales et al. (2017) show that there is very little mass contained in these objects: $\simeq$90 per cent of the total stellar mass in ETGs with masses $>10^8$ M$_\odot$ in the HRS volume is contained in the galaxies in the sample. As a result of the *Herschel* photometry (Ciesla et al. 2012; Smith et al. 2012b; Cortese et al. 2014) and the proximity of the galaxies, there are extremely sensitive measurements of the dust continuum emission in five far-infrared bands for each of the HRS galaxies. Even though ETGs are often assumed to contain very little dust, Smith et al. (2012b) detected continuum dust emission from 31 of the 62 HRS ETGs and obtained very tight limits on the amount of dust in the remainder.

High-quality photometry in 21 photometric bands, from the ultraviolet (UV) to the far-infared, makes the HRS ideal for the application of galaxy modelling programs such as MAGPHYS (Da Cunha, Charlot & Elbaz 2008). De Vis et al. (2017) applied MAGPHYS to the HRS galaxies, obtaining estimates of key galaxy properties such as star-formation rate and stellar mass. Eales et al. (2017) used these results to look at the relationship between specific star-formation rate and stellar mass in the HRS volume (Fig. 1), finding that galaxies follow a smooth curved Galaxy Sequence (GS), with a gradual change in galaxy morphology along the sequence and no abrupt change between LTGs and ETGs. They showed that the location and shape of the GS in Fig. 1 are consistent with other recent attempts either to plot the entire GS (Gavazzi et al. 2015) or to plot the part of the GS classified as star-forming (Renzini & Peng 2015). Oemler et al. (2017, O17) have recently carried out a reanalysis of the SDSS galaxy survey, taking account of several selection effects, and have found a galaxy distribution very like that in Fig. 1. Since Fig. 1 contains all the LTGs in the HRS volume with masses $\gtrsim 8 \times 10^8$ M$_\odot$, and since there is very little stellar mass in the ETGs in its bottom-left-hand corner, the diagram should be a good representation of where the stars in the Universe are today, after 12 billion years of galaxy evolution.

While the HRS was a sample of galaxies selected in the near-infrared, which were then observed in the far-infared with

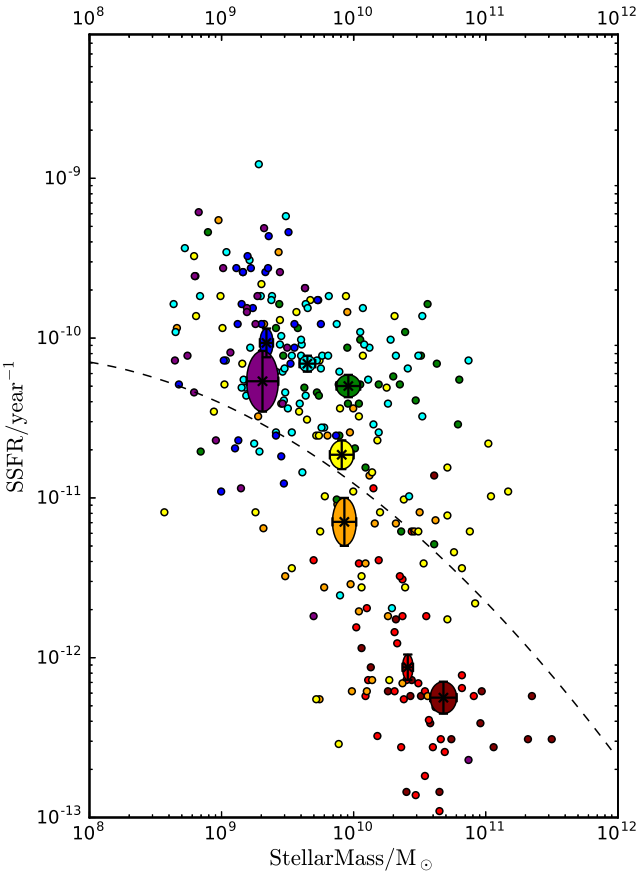

Figure 1. Specific star-formation rate versus stellar mass for the galaxies in the *Herschel* Reference Survey, a volume-limited sample designed to contain most of the stellar mass in the survey volume, reproduced from Eales et al. (2017; see that paper for more details). The colours show the morphologies of the galaxies: maroon – E and E/S0; red – S0; orange – S0a and Sa; yellow – Sab and Sb; green – Sbc; cyan – Sc and Scd; blue – Sd, Sdm; purple – I, I0, Sm and Im. The coloured ellipses show the 1σ error region on the mean position for each morphological class, with the colours being the same as for the individual galaxies. The dashed line shows the result of fitting a second-order polynomial to the H-ATLAS galaxies (Section 3), using a method that corrects for the effect of Malmquist bias. Note the consistency in where the GS lies, whether its location is obtained from a volume-limited survey such as the HRS or a far-infrared survey such as H-ATLAS.

Herschel, the H-ATLAS was a 'blind' far-infrared survey in which the galaxies were selected based on their far-infrared flux density. In its five fields the H-ATLAS detected ~500 000 sources. The fields we use in this paper are the three small fields on the celestial equator, which cover a total area of 161.6 square degrees and were the same fields surveyed in the Galaxy and Mass Assembly project (henceforth GAMA). GAMA was a deep spectroscopic survey (Driver et al. 2009; Liske et al. 2015) complemented with matched-aperture photometry throughout the *UV*, optical and infrared wavebands (Driver et al. 2016). We used the optical SDSS images to find the galaxies producing the *Herschel* sources and then the GAMA data to provide redshifts and matched-aperture photometry for these galaxies.

We have recently released our final images and catalogues for the GAMA fields (Bourne et al. 2016; Valiante et al. 2016[1]). The

[1] This dataset can be obtained from h-atlas.org

Table 1. The H-ATLAS base sample.

Redshift range	No.	ID fraction(%)	Last 0.5 mag(%)	Bad fits(%)	GAMA
$0.001 < z < 0.1$	3,456	91.3	0.7	12.1	17 768
$0.1 < z < 0.2$	7,096	87.7	5.1	7.1	38 768
$0.2 < z < 0.3$	5,400	80.4	22.3	9.2	21 323
$0.3 < z < 0.4$	3,604	72.2	39.5	12.8	7 289

Notes. Col. 1 – redshift range; col. 2 – No. of galaxies in base sample – these are the galaxies used in the analysis in this paper; col. 3 – estimated percentage of H-ATLAS sources in this redshift range for which our search procedure should have found the galaxies producing the submillimetre emission (Bourne et al. 2016); col. 4 – percentage of galaxies in column 2 with *r*-band magnitude in the range $19.3 < r < 19.8$ (see the text for significance); col. 5 – percentages that were excluded from the base sample because there was <1 per cent probability that the best-fitting MAGPHYS SED was a good fit to the multiwavelength photometry; col. 6 – no. of galaxies from the GAMA survey in this redshift range (Driver et al. 2009; Liske et al. 2015).

catalogue of *Herschel* sources (Valiante et al. 2016) contains 120 230 sources detected at $>4\sigma$ at 250, 350 or 500 μm, of which 113 995 were detected above this signal to noise at 250 μm, our most sensitive wavelength, which corresponds to a flux-density limit of $\simeq$30 mJy. We have also released a catalogue of 44 835 galaxies which are the probable sites of the *Herschel* sources (Bourne et al. 2016). We found these galaxies by looking for galaxies on the *r*-band SDSS images close to the positions of the *Herschel* sources; we then used the magnitude of the galaxy and its distance from the *Herschel* source to estimate a Bayesian probability (the 'reliability' in our nomenclature) that the galaxy is producing the far-infrared emission.

Our base sample in this paper consists of the 19 556 galaxies in this catalogue detected at $>4\sigma$ at 250 μm, with matched-aperture multiwavelength photometry and spectroscopic redshifts in the redshift range $0.001 < z < 0.4$, the lower redshift limit chosen to minimize the effect of galaxy peculiar motions. The redshift distribution of this sample is shown in Table 1.

There are several possible sources of error that we need to consider. The first is the possibility that we have incorrectly associated a *Herschel* source and an SDSS galaxy. We can estimate the number of sources that may have been misidentified in this way by adding up $1 - R$ for all the sources, where R is the reliability of the counterpart. We calculate that of our base sample, 435 sources (2.2 per cent) have been incorrectly associated with SDSS galaxies.

The second is that there are an additional 819 galaxies which satisfy the other criteria above but which do not have multiwavelength aperture-matched photometry, since their redshifts were measured after the completion of the GAMA photometry program. These are essentially random omissions from the sample and are thus very unlikely to have any effect on the results in Sections 3 and 4 (these objects are included in the investigation of the evolution of the luminosity function in Section 4.3).

A more important issue is the possibility that we have missed associations. Bourne et al. (2016) have estimated, as a function of source redshift, the probability that we will have found the galaxy producing the *Herschel* source. Their estimates are shown in Table 1, which range from 91.3 per cent in the redshift range $0.001 < z < 0.1$ to 72.2 per cent in the highest redshift bin, $0.3 < z < 0.4$.

The final source of error is the requirement that the galaxy has a spectroscopic redshift, which we have made so as not to introduce any additional errors into our spectral fits (Section 3). We can estimate the overall completeness of the base sample by finding the additional galaxies that have photometric redshifts in the redshift range $0.001 < z < 0.4$ but which do not have spectroscopic redshifts. There are 5701 of these galaxies, which implies that the spectroscopic sample is 78 per cent complete. However, we expect the completeness of the base sample to be a strong function of redshift. We investigated how the completeness varies with redshift using the following method. The magnitude limit of the GAMA spectroscopic survey was $r = 19.8$ (Liske et al. 2015). We can gauge the possibility that we have missed galaxies because they are fainter than this limit by counting the number of galaxies in the base sample that fall in the half magnitude *brighter* than the spectroscopic limit: $19.3 < r < 19.8$. If this number is small, we would not expect incompleteness from this effect to be an issue. We list these percentages in Table 1. In the lowest redshift bin, the percentage is very small (0.7 per cent), but it is very high in the two highest redshift bins. Therefore, the lowest-redshift bin should not be significantly affected but the two highest-redshift bins will be significantly incomplete. The incompleteness will be most severe for galaxies with low stellar masses.

In summary, there are a number of sources of systematic error associated with the method used to find the galaxies producing the *Herschel* sources. The numbers in Table 1 show that these errors are likely to be quite small for the lowest-redshift bin but large for the two highest-redshift bins, making the base sample highly incomplete at $z > 0.2$.

On top of these errors, there is the unavoidable selection effect found in all flux-density-limited surveys: Malmquist bias. The H-ATLAS is biased towards galaxies with high 250-μm luminosities in the same way that an optical survey such as the SDSS is biased towards galaxies with high optical luminosities. Thus galaxies with low masses of interstellar dust, such as ETGs, will be underrepresented in H-ATLAS. For example, the ETGs in the HRS have a mean dust mass of $\sim 10^5$ $M_\odot$ (Smith et al. 2012b), but there are only 22 galaxies in our base sample with dust-mass estimates (Section 3) less than $10^{5.5}$ $M_\odot$. In the next section, we will make an attempt to correct H-ATLAS for the effect of Malmquist bias.

The result of selection effects is that a very different galaxy population is found in a submillimetre survey such as H-ATLAS from an optical survey such as the SDSS. In optical colour-versus-absolute-magnitude diagrams, galaxies detected in optical surveys lie in a 'blue cloud' or on a 'red sequence' with a 'green valley' in between. We show in an accompanying paper (Eales et al. in preparation) that the distribution of H-ATLAS galaxies on the same diagram is almost the opposite of this, with the far-infared-selected galaxies forming a 'green mountain'. We show in the accompanying

paper that both distributions are the natural result of selection effects operating on the smooth GS shown in Fig. 1. In the next section, we start from our biased sample of galaxies detected in H-ATLAS[2] and investigate whether the GS we obtain after correcting for selection effects is consistent with the GS we see in Fig. 1.

3 THE H-ATLAS GALAXY SEQUENCE

3.1 Method

The main purpose of the work described in this section was to investigate whether the low-redshift GS derived from H-ATLAS, after correcting for selection effects, is consistent with the GS derived from the *Herschel* Reference Survey that is shown in Fig. 1. As for the HRS, we used MAGPHYS (Da Cunha et al. 2008) to estimate the specific star-formation rates and stellar masses of the galaxies in the base sample, which all have high-quality matched-aperture photometry in 21 bands from the UV, measured with the *Galaxy Evolution Explorer*, to the five *Herschel* measurements in the far-infrared.

For the reader who is not familiar with the model, we give here very brief details of the model and our application of it. MAGPHYS is a model of a galaxy based on the model of the ISM of Charlot & Fall (2000), who investigated the effects on a galaxy's spectrum and SED of the newly formed stars being more obscured by dust than the older stellar population, because they are still surrounded by the dust in their natal giant molecular clouds.

MAGPHYS generates 50 000 possible models of the SED of an unobscured stellar population, ultimately based on the stellar synthesis models of Bruzual & Charlot (2003), and 50 000 models of the dust emission from the interstellar medium. By linking the two sets of models using a dust obscuration model that balances the radiation absorbed at the shorter wavelengths with the energy emitted in the infrared, the program generates templates which are then fitted to the galaxy photometry. From the quality of the fits between the templates and the measurements, the program produces probability distributions for important global properties of each galaxy. An advantage of the model is that the large number of templates make it possible to generate a probability distribution for each galaxy property. MAGPHYS uses the stellar initial mass function from Chabrier (2003).

Our detailed procedure was the same, with the exceptions listed below, as that described by Smith et al. (2012a), who applied MAGPHYS to the galaxies in the small H-ATLAS field observed as part of the *Herschel* Science Demonstration Phase. As in the earlier paper, the value we use for each galaxy property is the median value from the probability distribution returned by MAGPHYS, since this is likely to be the most robust estimate (Smith et al. 2012a). The star-formation rate we use is the average star-formation rate over the last 0.1 Gyr.

The biggest change from the earlier work was that we replaced the UKIRT near-infrared photometry and *IRAS* photometry with the photometry in five near-infrared bands (z, Y, J, H and K_s) from the VISTA Kilo-Degree Infrared Galaxy Survey (VIKING; Edge et al. 2013) and in the four bands measured with the *Wide-Field Infrared Survey Explorer*. A minor change was in the calibration errors used for photometry measured with the two cameras on *Herschel*, PACS and SPIRE, which we reduced from the values used in our earlier paper to 5.5 per cent for SPIRE and 7 per cent for PACS, the values recommended by Valiante et al. (2016). We excluded galaxies from the base sample for which there was <1 per cent probability that the best-fitting MAGPHYS SED was a good fit to the multiwaveband photometry. The number of these objects is shown in Table 1. Smith et al. (2012a) did a detailed examination of these objects and concluded that the vast majority are due to serious problems with the aperture-matched photometry, probably due to neighbouring objects within the aperture. We have checked that none of the results in this paper is spuriously generated by the exclusion of these object by repeating the analysis with them included, obtaining similar results.

We have assumed that the SEDs are dominated by emission that is directly or indirectly from stars. This assumption is supported by the results of Marchetti et al. (2016), who, using *Spitzer* data, concluded that only $\simeq$3 per cent of the galaxies at $z < 0.5$ in the HerMES Wide sample, a *Herschel* sample with a similar depth to our own, have an SED dominated by emission from an AGN. Many of the H-ATLAS galaxies which do have an AGN-dominated SED will anyway have been eliminated by the requirement that MAGPHYS produces a good fit to the measured SED.

The results from MAGPHYS have been checked in a number of ways. Eales et al. (2017) showed that the MAGPHYS stellar mass estimates for the HRS galaxies agree well with the estimates of Cortese et al. (2012), who estimated stellar masses from i-band luminosities and a relation between mass-to-light ratio and g–i colour from Zibetti, Charlot & Rix (2009). In the same way, the MAGPHYS estimates of stellar mass for the H-ATLAS galaxies agree well with estimates from the optical spectral energy distributions (Taylor et al. 2011). We note, however, that these comparisons have been made with studies that are ultimately based on the same stellar synthesis models and initial mass function that MAGPHYS is based on.

We do not have independent measurements of the star-formation rate with which to test the MAGPHYS estimates. However, in a comparison of 12 different methods of estimating star-formation rates, Davies et al. (2016) showed that the use of MAGPHYS estimates does not lead to any biases in the relationship between SSFR and galaxy stellar mass (see their fig. 10).

Finally Hayward & Smith (2015) have demonstrated, using simulated galaxies, that MAGPHYS is very reliable for estimating galaxy stellar masses and star-formation rates, irrespective of star-formation history, viewing angle, black hole activity etc.

3.2 Results

Fig. 2 shows specific star-formation rate (SSFR) plotted against galaxy stellar mass for the H-ATLAS galaxies in four redshift bins. The errors in the estimates of the logarithm of SSFR are typically 0.2 but can be much larger for galaxies at the bottom of the diagram.

A simple argument shows one of the effects of Malmquist bias. The H-ATLAS galaxies are selected based on their continuum dust emission and thus the sample will be biased towards galaxies with a large mass of dust, and thus consequently a large ISM mass and a high star-formation rate. Since lines of constant star-formation rate run roughly parallel to the galaxy distributions in Fig. 2, the absence of galaxies to the bottom left of each panel may well be the result of Malmquist bias. Conversely, however, the upper envelope of each distribution, and its negative gradient, should not be significantly affected by this.

The distribution in the lowest redshift bin appears curved. To assess whether this is statistically significant, we fitted both a straight

[2] No more biased, of course, than an optical survey.

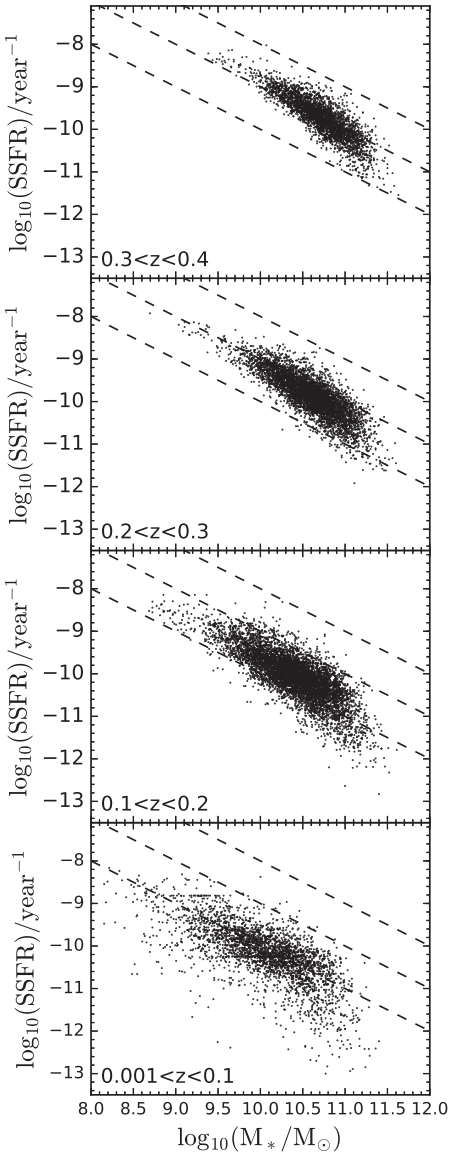

Figure 2. Specific star-formation rate versus galaxy stellar mass in four redshift bins. The three dashed lines correspond to star-formation rates of 1, 10 and 100 $M_\odot$ yr^{-1}.

line and a polynomial to the distribution, minimizing the sum of χ^2 in the SSFR direction. The polynomial had the form:

$$log_{10}(\mathrm{SSFR}) = a + b \times (\log_{10} M_* - 10.0) + c \times (\log_{10} M_* - 10.0)^2 \quad (1)$$

The best-fitting polynomial is shown in Fig. 3. The reduction in the total value of χ^2 obtained from using a polynomical rather than a straight line is 336. Since the expected reduction in χ^2 when fitting a function with one additional parameter is itself distributed as χ^2 with 1 degree of freedom, the reduction in χ^2, and thus the curvature in the low-redshift GS, is highly significant. This adds to the other recent evidence that the GS is curved, whether only star-forming galaxies are plotted (Whitaker et al. 2014; Lee et al. 2015; Schreiber et al. 2016; Tomczak et al. 2016) or all galaxies are plotted (Gavazzi et al. 2015; Oemler et al. 2017 – henceforth O17).

We used the following method to correct for the effect of Malmquest bias in Fig. 3. We divided the SSFR-versus-stellar-mass

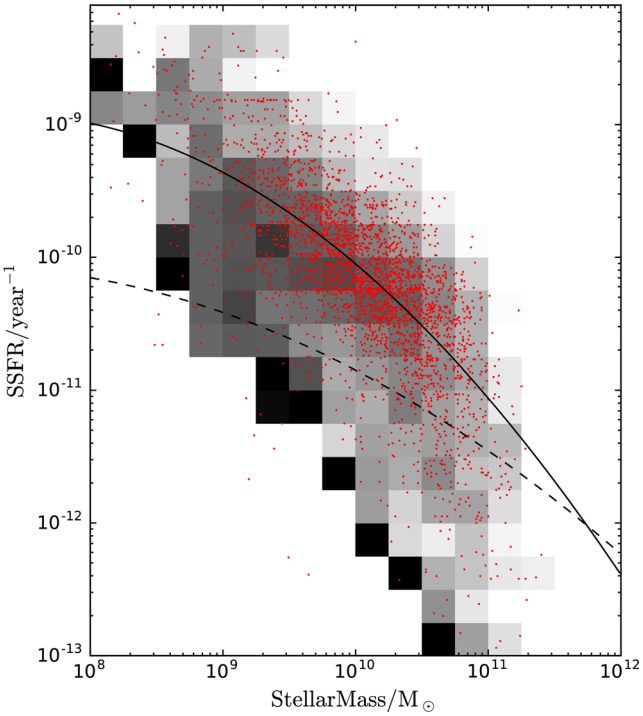

Figure 3. Specific star-formation rate versus galaxy stellar mass for the H-ATLAS galaxies in the redshift range $0.001 < z < 0.1$. The red points show the positions of the H-ATLAS galaxies. The grey-scale shows how the number-density of H-ATLAS galaxies varies over the diagram after making a correction for the effect of accessible volume (see the text). The solid black line shows the best-fitting second-order polynomial to the raw data points; the dashed line shows the fit when the data points are weighted by 1/accessible volume. The form of the polynomial is $\log_{10}(\mathrm{SSFR}) = \mathrm{a} + \mathrm{b} \times (\log_{10}\mathrm{M}_* - 10.0) + \mathrm{c} \times (\log_{10}\mathrm{M}_* - 10.0)^2$. For the raw data points the values of *a*, *b* and *c* are −10.05, −0.85 and −0.16, respectively, and for the weighted points the values are −10.85, −0.52 and −0.09, respectively.

diagram into rectangular bins and calculated the following quantity in each bin:

$$N(\mathrm{SSFR}, M_*) = \sum_i \frac{1}{V_{\mathrm{acc},i}} \quad (2)$$

where the sum is over all the galaxies in that bin and $V_{\mathrm{acc},i}$ is the accessible volume of the i'th galaxy, the volume in which that galaxy could still have been detected above the 250-μm flux limit. This is given by:

$$V_{\mathrm{acc},i} = \int_{z_{\mathrm{min}}}^{z_{\mathrm{max}}} \mathrm{d}V \quad (3)$$

In this equation, z_{min} is the lower redshift limit (0.001) and z_{max} is the lower of (a) the upper redshift limit of the redshift bin and (b) the redshift at which the flux density of the galaxy would equal the 250-μm flux limit of the sample.

This technique is the standard technique for correcting the effect of accessible volume. It will produce an unbiased estimate of $N(\mathrm{SSFR}, M_*)$ as long as there are representatives of all kinds of galaxy in the sample. We have applied it to the lowest redshift bin because the low lower redshift limit (0.001) means that there are galaxies with very low dust masses in the sample, which is not the case for the higher redshift bins. However, even if the answer is unbiased, it will be very noisy if there are only a few representatives of a class, which is the case for galaxies with the dust masses typical of ETGs (Section 2). This indeed is what we see in Fig. 3,

where N(SSFR, M_*) is shown as a grey-scale. The distribution, after it has been corrected for Malmquist bias, is clearly very noisy but lies, as expected, well below the observed distribution. Note that this reconstructed GS is particularly noisy at the lower right-hand end because of the small number of ETGs detected in H-ATLAS (Section 2).

We fitted the polynomial in equation (1) to the data points again, this time weighting each point by $1/V_{\rm acc}$ in order to correct for the effect of Malmquist bias. The dashed black line in Fig. 3 shows the best-fitting polynomial. As expected, it lies well below the polynomial that is the best fit to the unscaled data points. We have also plotted this Malmquist-bias-corrected line on to Fig. 1, which shows the GS derived from the HRS. Without being a particularly good fit, the line passes through the middle of the HRS points, showing that the GS derived from a volume-limited survey and the GS derived from correcting a far-infrared survey for Malmquist bias are consistent. In an earlier paper we showed that the GS from the HRS is consistent with the low-redshift GS derived using other methods (Eales et al. 2017), and the results from this section show that the GS derived from two very different *Herschel* surveys are also in reasonable agreement.

In the remainder of this section we describe some analysis whose original goal was to test our method for correcting Malmquist bias but which turned out to have an unexpected and interesting result. We originally decided to test the method by using it to estimate the stellar mass function for star-forming galaxies, which we could then compare with the same stellar mass function derived from optical surveys.

We estimated the stellar mass function from the H-ATLAS galaxies in each redshift bin using the following formula:

$$\phi(M_*){\rm d}M = \sum_i \frac{1}{V_{{\rm acc},i}} \tag{4}$$

In this formula, the sum is over all galaxies with $M_* < M_i < M_* + {\rm d}M$, and $V_{{\rm acc},\,i}$ is the accessible volume of each galaxy (equation 2).

After estimating the stellar mass function from the H-ATLAS data, we then calculated:

$$f = \frac{(\phi(M_*))_{\rm submm}}{(\phi(M_*))_{\rm optical}} \tag{5}$$

in which the numerator is the stellar mass function derived from the H-ATLAS galaxies using equation (4) and the denominator is the stellar mass function for star-forming galaxies derived from optical samples; for the latter, at $z < 0.2$ we used the mass function from Baldry et al. (2012) and at $z > 0.2$ we used the mass function for $0.2 < z < 0.5$ derived by Ilbert et al. (2013).

Fig. 4 shows f plotted against stellar mass for the four redshift bins. For the two highest redshift bins, the value of f is much less than 1, showing that at $z > 0.2$, even after correcting for accessible volume, we are missing a large fraction of star-forming galaxies. This result is not unexpected because we showed in Section 2 that the base sample is seriously incomplete in these bins.

In the second lowest redshift bin ($0.1 < z < 0.2$), the H-ATLAS mass function is incomplete at stellar masses of $<10^{10}\,{\rm M}_\odot$, and in the lowest redshift bin it is incomplete at stellar masses of $<10^{9}\,{\rm M}_\odot$. Above these stellar masses, however, f reaches values that are much greater than 1, reaching values of 3–5 at the highest stellar masses. At first sight, this result suggests that a far-infrared survey is actually much better at finding star-forming galaxies than an optical survey, with optical surveys missing a population of star-forming galaxies. We will investigate this result further in the following section.

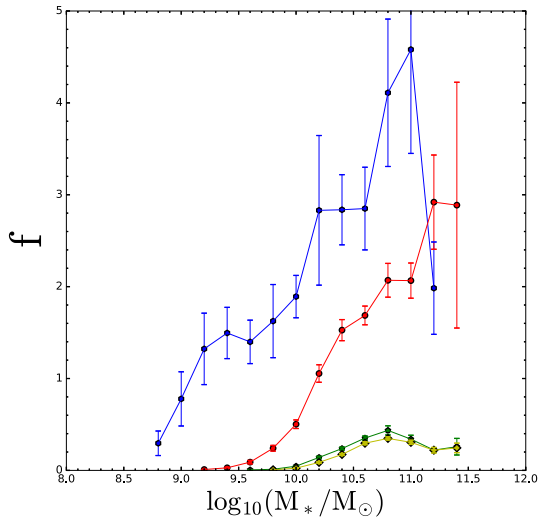

Figure 4. The ratio of the galaxy stellar mass function derived from H-ATLAS to that derived from optical surveys plotted against galaxy stellar mass for four redshift bins: $0.001 < z < 0.1$ – blue symbols; $0.1 < z < 0.2$ – red symbols; $0.2 < z < 0.3$ – green symbols; $0.3 < z < 0.4$ – light green symbols.

4 RED AND BLUE GALAXIES AS SEEN BY *Herschel*

4.1 The galaxy sequence

In the comparison of the stellar mass functions at the end of the previous section, we implicitly assumed that the galaxies detected by H-ATLAS are star-forming galaxies. However, there is intriguing evidence that *Herschel* surveys do also detect a population of galaxies that have red colours (Dariush et al. 2011, 2016; Rowlands et al. 2012; Agius et al. 2013). These red colours might indicate a galaxy with an old stellar population or a star-forming galaxy with colours reddened by dust. In this section and the next one, we step back from our previous assumption about the kind of galaxy that should be detected by a far-infrared survey; instead, we use the optical colours and spectra of the galaxies to determine empirically what kinds of galaxy are actually detected.

In our investigation, we have used the optical colours to separate the H-ATLAS galaxies into two classes using two alternative criteria from Baldry et al. (2012). Baldry et al. called these classes 'star-forming' and 'passive', but we will call them 'blue' and 'red', since the former nomenclature makes the assumption that red galaxies are not forming stars. As the first criterion we use the rest-frame $g - r$ colour of the galaxy to classify it as red or blue using the dividing line on the colour versus absolute magnitude diagram:

$$g - r = -0.0311 M_r + 0.0344 \tag{6}$$

As the second criterion we use the rest-frame $u - r$ colour with the dividing line on the colour versus absolute magnitude diagram being:

$$u - r = 2.06 - 0.244 \tanh\left(\frac{M_r + 20.07}{1.09}\right) \tag{7}$$

We calculated the rest-frame colours by calculating individual k-corrections for each galaxy by applying $KCORRECT$ $v4\_2$ (Blanton et al. 2003; Blanton & Roweis 2007). In brief, this package finds the linear combination of five template spectra that gives the best fit to the five SDSS magnitudes for each galaxy and then uses

Table 2. Percentages of red galaxies in H-ATLAS.

Redshift	$(g-r)(\%)$	$(u-r)(\%)$	$(g-r)$ plus evolution(%)	$(u-r)$ plus evolution(%)
$0.001 < z < 0.1$	27	16	29	18
$0.1 < z < 0.2$	26	15	31	18
$0.2 < z < 0.3$	24	18	33	23
$0.3 < z < 0.4$	21	21	35	28

Notes. The percentage of H-ATLAS galaxies in different redshift ranges classified as red using equation (6) (columns 2 and 4) and equation (7) (columns 3 and 5). In columns 4 and 5, we add a correction to equations 6 and 7 to allow for the expected evolution of a very old stellar population (see the text).

this model to calculate the *K*-correction for the galaxy (Blanton & Roweis 2007). Some additional details of the implementation of the code are given in Loveday et al. (2012).

Equations (6) and (7) were determined by Baldry et al. (2012) from the low-redshift galaxy population. However, even a galaxy today in which no stars have formed for the last 10 billion years will have had bluer colours in the past because of the evolution in the turn-off mass on the stellar main sequence. We therefore investigated the effect of adding a small correction to these equations to model the expected evolution in the colours of a very old stellar population. Our model of this effect was based on a model of a single stellar population from Bruzual & Charlot (2003) with a Salpeter initial mass function and solar metallicty. We assumed that the galaxy started forming 12 Gyr ago with the star-formation rate proportional to $\exp(-t/\tau)$ and $\tau = 1$ Gyr.

Table 2 gives the percentages of red galaxies in the different redshift bins for the two colour criteria and also shows the effect of adding the evolutionary correction. Rather surprisingly, even without making the evolutionary correction, $\simeq$15–30 per cent of the H-ATLAS galaxies are red galaxies. This is higher than the value of $\simeq$4.2 per cent found by Dariush et al. (2016) for H-ATLAS galaxies at $z < 0.2$. We suspect that the difference arises because Dariush et al. used optical-UV colours rather than optical colours, a suspicion we will explain in the next section (Section 4.2). Fig. 5 shows the GS again, but this time with the points colour-coded to show which galaxies are red and blue according to equation (6) (equation 7 produces a very similar figure).

The significant fraction of red galaxies explains the values of $f > 1$ in Fig. 4, because these galaxies would have been classified as passive galaxies using optical criteria and so would have been omitted from the mass function for star-forming galaxies derived from optical surveys. However, these red galaxies still have significant reservoirs of interstellar gas (after all, they are detected because of the continuum emission from interstellar dust) and the MAGPHYS results imply they are still forming stars. We will investigate further the properties of this interesting population in the next section. Figs 5 is a striking demonstration of why the GMS produced from a subset of galaxies classified as star-forming will generally be flatter than the GS we have derived from the two *Herschel* surveys. Imagine removing all the red galaxies in Figs 5; the GMS would then have a much flatter slope.

Although there are fewer optically red galaxies than optically blue galaxies in H-ATLAS, a simple argument shows that optically red star-forming galaxies are not a peripheral population. The optically red galaxies are underrepresented in H-ATLAS because of Malmquist bias. At a given stellar mass, Fig. 5 shows that optically red galaxies generally have lower values of SSFR than optically blue galaxies, which in turn means a lower star-formation rate and, through the Kennicutt–Schmidt law, a lower gas and dust mass – leading to a smaller accessible volume and Malmquist bias. Fig. 4, where we have attempted to correct for Malmquist bias, shows this quantitatively. The implication of that figure is that, at a given stellar mass, the space-density of optically red star-forming galaxies is at least as high as that of optically blue star-forming galaxies.

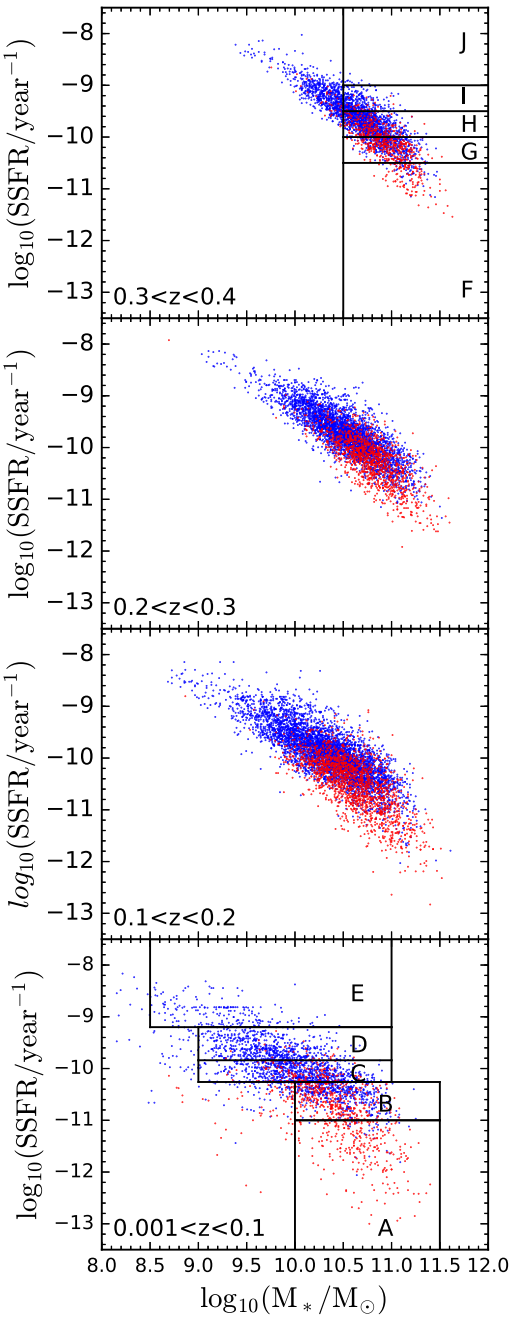

Figure 5. Specific star-formation rate versus stellar mass in the four redshift bins. Red points and blue points show galaxies that have redder and bluer rest-frame $g - r$ colours, respectively, than the colour defined by equation (6). The boxes show the ranges of SSFR and stellar mass used to produce the stacked spectra shown in Figs 6 and 7 (Section 4.2) (use the letter in the box to find the corresponding spectrum).

Optical investigators have generally missed this population by classifying these galaxies as passive. However, they do have the following excuse. A comparison of the stellar mass functions given by Baldry et al. (2012; their fig. 15) for star-forming galaxies and

passive galaxies (precisely equivalent to our optically blue and optically red classes) shows that the space density of the two galaxy types is the same at a stellar mass of $\simeq 10^{10}\,M_{\odot}$, but that at higher stellar masses the space-density of passive galaxies is higher, with a maximum difference of a factor of $\simeq 5$ at a stellar mass of $\simeq 4 \times 10^{10}\,M_{\odot}$. Given the much larger number of passive galaxies, even a small change in how one divides galaxies into the passive and star-forming classes will have a large effect on estimates of the space-density of star-forming galaxies.

Not all optical investigators, however, have missed this population. In their elegant reanalysis of the SDSS galaxy sample, O17 showed that there is an intermediate population of galaxies between those that are rapidly forming stars and passive galaxies. The galaxies in this intermediate class are still forming stars and seem identical to our optically red star-forming galaxies. O17 conclude that at a given stellar mass the number of galaxies in this intermediate class is roughly the same as the number in the rapidly star-forming class, thus reaching exactly the same conclusion as we do but starting from a traditional optical survey.

4.2 Stacking spectra – the nature of the red and blue galaxies

The colours of the optically-red H-ATLAS galaxies might indicate an old stellar population or alternatively a star-forming galaxy whose colours are reddened by dust. We attempted to distinguish between these possibilities using the galaxies' spectra. The spectra come from the GAMA and SDSS projects, with most of the spectra coming from the former. Hopkins et al. (2013) describe the calibration and other technical details of the GAMA spectra. The GAMA project used the AAOmega spectrograph on the AAT, which has fibres with an angular diameter on the sky of 2 arcsec. This corresponds to a physical size at redshifts of 0.1, 0.2, 0.3 and 0.4 of 3.6, 6.6, 8.9 and 10.7 kpc, respectively.

We divided the SSFR versus stellar mass diagrams for the H-ATLAS galaxies with $0.001 < z < 0.1$ and with $0.3 < z < 0.4$ each into five boxes, which are shown in the bottom and top panels of Fig. 5. We then calculated the median rest-frame spectrum of all the GAMA and SDSS spectra in each box (Figs 6 and 7). We measured the equivalent width of the Hα line from each median spectrum, using the wavelength range $6555.5 < \lambda < 6574.9$ Å to measure the flux in the line and the wavelength ranges $6602.5 < \lambda < 6622.5$ Å and $6509.5 < \lambda < 6529.5$ Å to estimate the mean value of the continuum at the line wavelength. The Hα equivalent width, the ranges of stellar mass and SSFR for each box and the number of galaxies in the box are shown by the side of each spectrum in Figs 6 and 7.

First, let us consider the stacked spectra for the low-redshift galaxies (Fig. 6). The galaxies in the bottom box in Fig. 5 almost all have red optical colours. The stacked spectrum for this box, which is shown in the lowest panel in Fig. 6, is strongly characteristic of an old stellar population. The red colours are therefore generally the result of the age of the stellar population rather than dust reddening.

This figure gives further insights into why different studies of the GMS can find very different results. As we move down the panels in Fig. 6, the appearance of the stacked spectra gradually changes, with the equivalent width of the Hα line, the brightest emission line in the spectra, steadily decreasing. This is not surprising (although it is reassuring) because the luminosity of the Hα line is often used to estimate a galaxy's star-formation rate (Davies et al. 2016; Wang et al. 2016b). When the Hα line is used in studies of the GMS to separate star-forming from passive galaxies, the dividing line is usually an Hα equivalent width in the range $3 < EW < 10$ Å (Bauer et al. 2013; Casado et al. 2015). The equivalent width of Hα in the

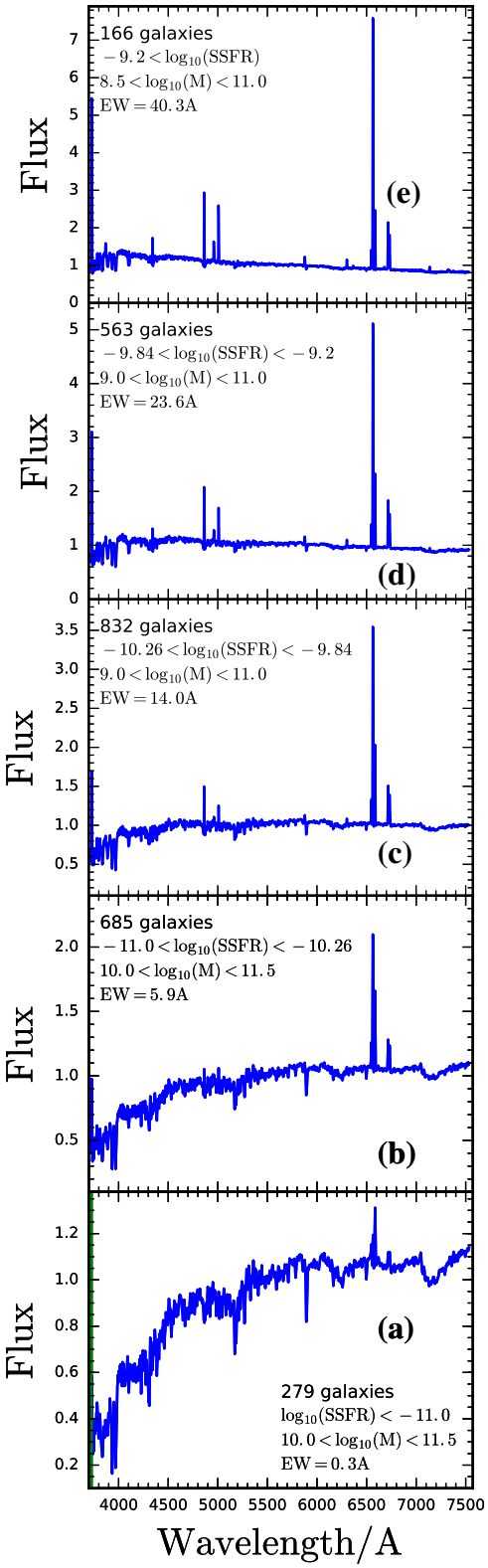

Figure 6. Median rest-frame spectra of galaxies in the redshift range $0.001 < z < 0.1$ in the five boxes shown in the bottom panel of Fig. 5 (use the letter to find the box). The ranges of stellar mass and SSFR for each box are given by the spectrum. Note (a) how, as one moves down the panels to lower values of SSFR, the equivalent width of the Hα line also decreases and (b) how the red optical colours of the galaxies in the bottom box in Fig. 5 are clearly caused by an old stellar population rather than by reddening by dust.

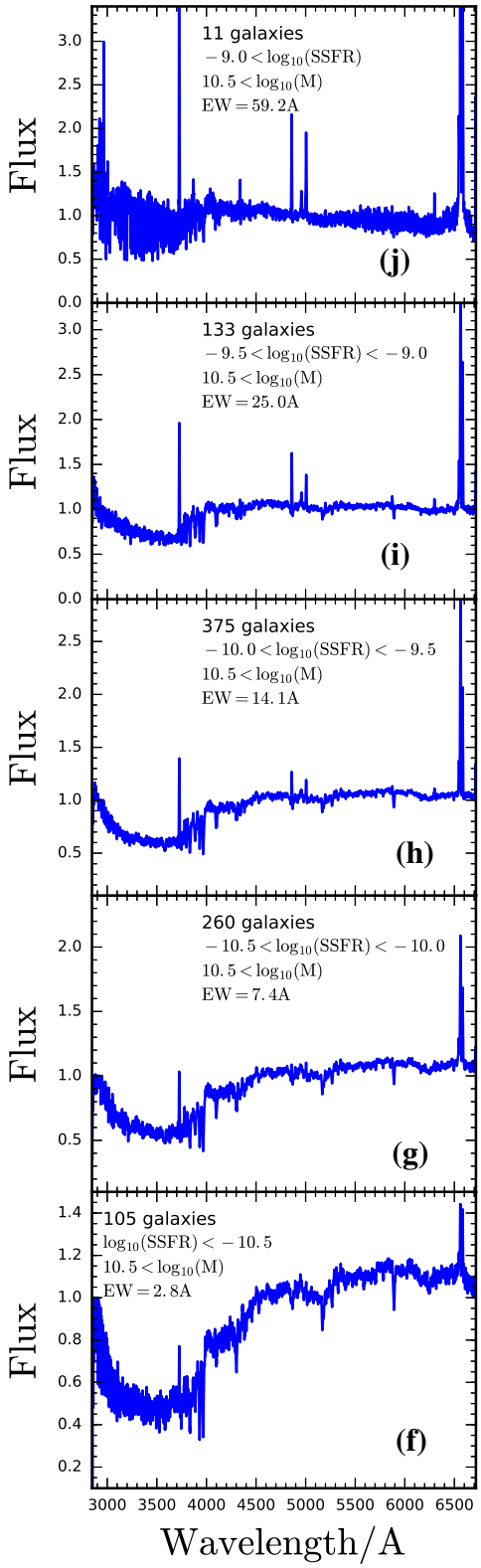

Figure 7. Median rest-frame spectra of galaxies in the redshift range $0.3 < z < 0.4$ in the five boxes shown in the top panel of Fig. 5 (use the letter by the spectrum to find the box). The ranges of stellar mass and SSFR for each box are given by the spectrum. Note how the spectra have both a clear 4000 Å break, showing the existence of an old stellar population, and strong Hα emission and a *UV* upturn, indicating a high star-formation rate.

three lowest boxes in Fig. 6 is, in order of increasing SSFR, 0.3, 5.9 and 14.0 Å. Therefore, when this method is used to separate star-forming and passive galaxies, the shape of the GMS that is found depends critically on the exact value of the equivalent width used to divide the galaxies.

These results also suggest something more fundamental which we will return to later. Whereas the optical view of the galaxy population is that there are two distinct classes of galaxy (Section 1), the *Herschel* results show more continuity. The red galaxies have colours and stacked spectra that imply they have old stellar populations but their detection by *Herschel* shows they contain a substantial ISM – and both our MAGPHYS results and the Hα equivalent widths imply they are still forming stars. Furthermore, the overlap of red and blue galaxies in Fig. 5 also implies that the two classes are not clearly physically distinct.

The blurring between the two classes is even more evident when we turn to the high-redshift population. In Fig. 7 we show the result of stacking the spectra of the galaxies in the redshift range $0.3 < z < 0.4$ and for $\log_{10}(M/\mathrm{M}_{\odot}) > 10.5$. The base sample is highly incomplete in this redshift range, although the incompleteness is most severe at lower stellar masses (Section 2). The stacked spectra for this high-redshift bin are visually quite startling because they all show clear evidence of both an old and a young stellar population. In all the stacked spectra, there is a clear 4000 Å break, evidence of an old stellar population. Since the SDSS *u*-band is centred at $\simeq$3500 Å, the existence of the 4000 Å break immediately explains why so many of the galaxies fall into the optically red class. However, in all the stacked spectra there are also clear signs of a high star-formation rate, including strong emission lines, in particular Hα, and a *UV* upturn. We do not know whether this *UV* upturn is present in the galaxies in the low-redshift bin because our spectra for this bin (Fig. 6) do not extend to a low enough rest-frame wavelength, but a *UV* upturn would explain why Dariush et al. (2016) found a much smaller fraction of red galaxies when using the *UV*-optical colours to classify the galaxies.

Fig. 7 shows that the rapid low-redshift evolution that we have seen in previous H-ATLAS studies (Section 1) is caused by galaxies with high stellar masses and a large population of old stars. In the Universe today, galaxies like this are forming stars at a very low rate but 4 billion years back in time they were clearly forming stars at a much faster rate.

4.3 The evolution of the red and blue galaxies

In earlier papers (Dye et al. 2010; Wang et al. 2016a), we showed that the H-ATLAS 250-μm luminosity function shows rapid evolution over the redshift range $0 < z < 0.4$ with significant evolution even by a redshift of 0.1. Marchetti et al. (2016) found similar results from an analysis of the results of the other large *Herschel* extragalactic survey, HerMES. In this section we consider the evolution of the 250-μm luminosity function separately for red and blue galaxies.

In this case we started with *all* the galaxies from the GAMA fields detected at $>4\sigma$ at 250 μm with spectroscopic (by preference) or photometric redshifts in the range $0.001 < z < 0.4$ (Bourne et al. 2016; Valiante et al. 2016). Of the 25,973 H-ATLAS galaxie in this sample, 20,012 have spectroscopic redshifts. We used the $u - r$ colour criterion (equation 7) to divide the H-ATLAS galaxies into red and blue galaxies, although the results using the $g - r$ colour criterion (equation 6) were very similar. We made the small correction to equation (7) that allows for the fact that the colours of

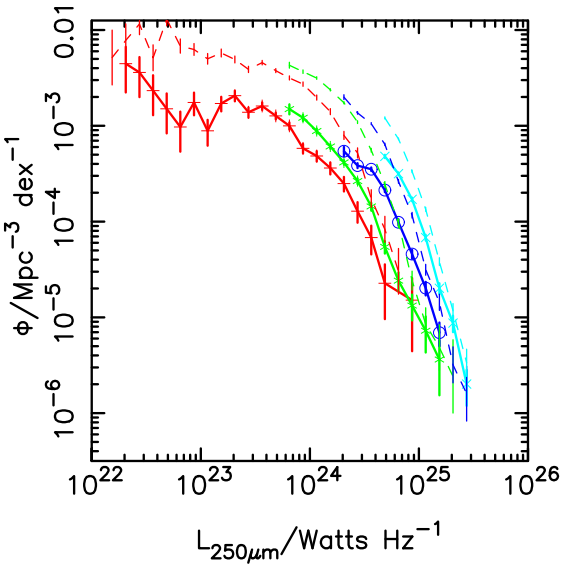

Figure 8. The 250-μm luminosity functions for the optically red H-ATLAS galaxies (solid lines) and optically blue H-ATLAS galaxies (dashed lines). The colours correspond to the following redshift ranges: red – $0 < z < 0.1$; green – $0.1 < z < 0.2$; dark blue – $0.2 < z < 0.3$; light blue – $0.3 < z < 0.4$.

even a very old stellar population must have been redder in the past (Section 4.1), although this actually makes very little difference to the results.

To calculate the luminosity function for each class, we used the estimator invented by Page & Carerra (2000), since this has some advantages for submillimetre surveys (Eales et al. 2009):

$$\phi(L_1 < L < L_2, z_1 < z < z_2)\Delta\log_{10}L\Delta z = n/V \quad (8)$$

in which n is the number of galaxies in this bin of luminosity and redshift and V is the accessible volume averaged over the luminosity range of this bin. We multiplied the luminosity function in each redshift bin by $1/C$, where C is the estimated efficiency of our method for finding the galaxies producing the far-infrared emission (Bourne et al. 2016; column 3 of Table 1).

Fig. 8 shows the luminosity function for the optically red and optically blue galaxies. Strong evolution is seen in the luminosity function for both populations, with the evolution in the red population looking slightly stronger. We quantified the evolution by fitting a Schechter function to each empirical luminosity function. For the lowest-redshift luminosity function, we allowed all three parameters of the Schechter function – α, L_* and ϕ_* – to vary. For the other luminosity functions, which have a smaller range of luminosity, we only allowed L_* and ϕ_* to vary, using the value of α from the low-redshift bin. We then used the estimates of the parameters at each redshift to investigate the evolution of ϕ_* and L_*. We assumed that the evolution has the form $\phi_* = \phi_{*0}(1+z)^n$ and $L_* = L_{*0}(1+z)^m$. We found $n = 0.24 \pm 0.04$ and $m = 3.69 \pm 0.01$ for the optically blue galaxies and $n = 3.66 \pm 0.06$ and $m = 1.86 \pm 0.01$ for the optically red galaxies. Therefore, there is strong evolution in L_* and ϕ_* for the red galaxies and strong evolution in L_* for the blue galaxies.

Bourne et al. (2012) also found evidence for evolution in submillimetre luminosity and dust mass for both red and blue galaxies, with marginal evidence of stronger evolution for the red galaxies. The stacking analysis of Bourne et al. was carried out on an optically selected sample of galaxies, and is therefore evidence that the strong evolution we see for optically red galaxies is not just a phenomenon associated with an interesting, but ultimately unimportant population detected by *Herschel*, but applies to the whole galaxy population.

4.4 How star-formation efficiency varies along the GS

Results from the *Herschel* Reference Survey show that galaxy morphology changes gradually along the GS, the morphologies moving to earlier types on the Hubble sequence as one moves down the GS (Fig. 1; Eales et al. 2017). This progression implies an increase in the bulge-to-disc ratio which, Martig et al. (2009) have argued should lead to a decrease in star-formation efficiency (SFE, star-formation rate divided by ISM mass). In this section we test this hypothesis by investigating whether SFE varies along the GS. There is already some evidence from other surveys that SFE and SSFR are correlated (Saintonge et al. 2012; Genzel et al. 2015).

We have restricted our analysis to the H-ATLAS galaxies in the redshift range $0.001 < z < 0.1$. In our analysis we use the MAGPHYS estimates of the star-formation rate and the dust mass, using the dust mass of each galaxy to estimate the mass of the ISM. Many authors (Eales et al. 2012; Scoville et al. 2014; Genzel et al. 2015; Groves et al. 2015) have argued this is a better way of estimating the ISM mass than the standard method of using the 21-cm and CO lines because of the many problems with CO, in particular the evidence that one third of the molecular gas in the Galaxy contains no CO (Abdo et al. 2010; Pineda et al. 2013; Planck Collaboration 2011), which is probably because of photo-disintegration of the CO molecule. Dust grains, on the other hand, are quite robust, and the main problem with the dust method is the fact that the dust-to-gas ratio is likely to depend on metallicity, a problem of course that is shared by the CO method.

There is a lot of evidence that above a transition metallicity ($12 + \log(\mathrm{O/H}) \simeq 8.0$) the dust-to-gas ratio is proportional to the metallicity (James et al. 2002; Draine et al. 2007; Bendo et al. 2010; Smith et al. 2012c; Sandstrom et al. 2013; Rémy-Ruyer et al. 2014). In order to test how robust our results are to the metallicity correction, we have used three different methods for doing this correction. In the first method we make no correction for metallicity and assume that each galaxy has a dust-to-gas ratio of 0.01. In the second method we estimate the metallity of each galaxy from its stellar mass using the relationship found by Tremonti et al. (2004):

$$12 + \log_{10}(O/H) = -1.492 + 1.847(\log_{10}M_*) - 0.08026(\log_{10}M_*)^2 \quad (9)$$

We then assume that the dust-to-gas ratio is proportional to the metallicity and that a galaxy with solar metallicity has a dust-to-gas ratio of 0.01. The third method is the same as the second except that we use the relationship found by Hughes et al. (2013) from their study of HRS galaxies:

$$12 + \log_{10}(O/H) = 22.8 - 4.821(\log_{10}M_*) + 0.519(\log_{10}M_*)^2 - 0.018(\log_{10}M_*)^3 \quad (10)$$

The obvious statistical test is to see whether there is any correlation between SFE and SSFR. However, this is dangerous because both quantities are ratios with the star-formation rate in the numerator; thus errors in the star-formation-rate estimates may lead to a spurious correlation. Instead, we have compared the SFE of the optically red and optically blue galaxies, since this classification was done without using any of the MAGPHYS estimates and yet

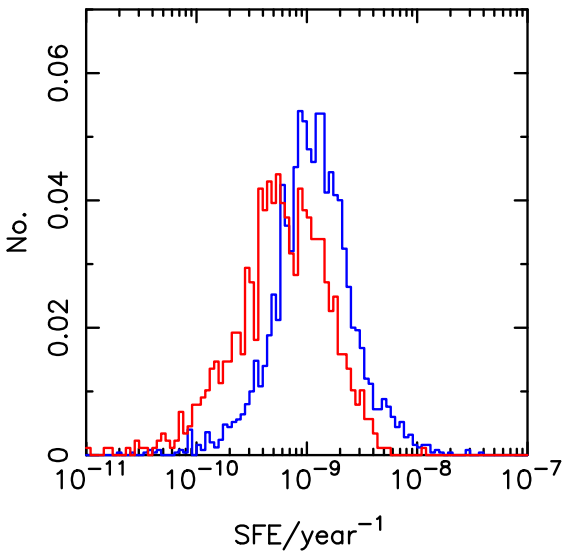

Figure 9. Histograms of star-formation efficiency for the optically red galaxies (red line) and optically blue galaxies (blue line) for the H-ATLAS galaxies in the redshift range $0.001 < z < 0.1$. In this diagram, we have used the g-r colour and equation 6 to split the galaxies into the two classes and the metallicity relationship of Tremonti et al. (2004) to correct for the metallicity effect (see the text). The histograms have been normalized so that the areas under both are the same.

we know from Fig. 5 that optically red galaxies have lower SSFR values than optically blue galaxies.

Fig. 9 shows the distributions of SFE for the optically red and optically blue galaxies when the metallicity correction is made using equation (9). The figures produced using the two other methods look very similar. The mean values of SFE for the optically red and optically blue galaxies are given in Table 3, for all three metallicity-correction methods and for both methods of classifying the galaxies as red or blue. In each case, we have compared the two distributions using the two-sample Kolmogorov–Smirnov (KS) test, testing the null hypothesis that the two samples are drawn from the same population. The values of the KS statistic and the probabilities that the two samples are drawn from the same population are given in Table 3.

The KS test shows that for all six variations on the basic method the probability that the star-formation efficiency of the optically red and optically blue galaxies are the same as < 0.1 per cent. Table 3 shows that the mean SFE of the optically red galaxies is lower by a factor of $\simeq$1.9–2.9 than the optically blue galaxies. Saintonge et al. (2012) found that as the SSFR decreases by a factor of $\simeq$50, SFE decreases by a factor of $\simeq$4 (see their fig. 2). The shift in SSFR between the optically blue and optically red galaxies in Fig. 5 is a little less than this and so our result seems to be in reasonable agreement with their result.

5 DISCUSSION

5.1 What have we learned from *Herschel*?

We have learned three main things from the *Herschel* extragalactic surveys that need to be explained by any comprehensive theory of galaxy evolution.

We have learned first that the galaxy population shows rapid evolution at a surprisingly low redshift. This is evident in the sub-millimetre luminosity function (Dye et al. 2010; Wang et al. 2016a), the dust masses of galaxies (Dunne et al. 2011; Bourne et al. 2012) and the star-formation rates, whether estimated from radio continuum observations (Hardcastle et al. 2016) or from bolometric dust emission (Marchetti et al. 2016). The rapid evolution in dust mass and star-formation rate are of course connected, since stars form out of gas and the dust traces the interstellar gas reservoir.

Several recent studies have found that the GS is curved, whether only star-forming galaxies are plotted (Whitaker et al. 2014; Lee et al. 2015; Schreiber et al. 2016; Tomczak et al. 2016) or all galaxies are plotted (Gavazzi et al. 2015; O17). The results from the two *Herschel* surveys confirm and extend this result. Both the *Herschel* surveys, selected in very different ways, show that galaxies lie on an extended curved GS rather than a star-forming GMS and a separate region of 'passive' or 'red-and-dead' galaxies (Figs 1 and 3). The GS shown in Figs 1 and 3 extends down to lower values of SSFR than most of the other studies because we have made no attempt to remove 'passive' galaxies, a distinction which we argue below is anyway rather meaningless.

Third, we have learned that the operational division often used in optical studies between red and blue galaxies looks distinctly arbitrary when viewed from a submillimetre perspective. 15–30 per cent of the H-ATLAS galaxies fall into the red category, but these galaxies clearly are not quenched or passive galaxies, since they still have large reservoirs of interstellar material and are still forming stars.

Table 3. The star-formation efficiency of optically red and optically blue galaxies.

Colour	Metallicity correction	$n_{\rm red}$	$n_{\rm blue}$	$< {\rm SFE}_{\rm red} >$	$< SFE_{\rm blue} >$	KS	Prob.(%)
$g-r$	None	885	2502	-9.59 ± 0.01	-9.19 ± 0.01	0.40	<0.1
$g-r$	Tremonti	885	2502	-9.24 ± 0.01	-8.95 ± 0.01	0.31	<0.1
$g-r$	Hughes	885	2502	-9.74 ± 0.01	-9.41 ± 0.01	0.35	<0.1
$u-r$	None	534	2853	-9.68 ± 0.02	-9.22 ± 0.01	0.43	<0.1
$u-r$	Tremonti	534	2853	-9.33 ± 0.02	-8.97 ± 0.01	0.38	<0.1
$u-r$	Hughes	534	2853	-9.84 ± 0.02	-9.43 ± 0.01	0.42	<0.1

Notes. The columns are as follows: Col. 1 – the colour used to divide galaxies into optically red and optically blue galaxies; col. 2 – the method used to correct the dust-to-gas ratio for the effect of metallicity (see the text for details); col. 3 – the number of optically red galaxies; col. 4 – the number of optically blue galaxies; col. 5 – the mean value of the logarithm of star-formation efficiency for the optically red galaxies; col. 6 – the mean value of the logarithm of star-formation efficiency for the optically blue galaxies; col. 7 – the value of the two-sample KS statistic used to compare the SFE distributions of the optically red and optically blue galaxies; col. 8 – the probability that such a high value of the KS statistic would be obtained if the two distributions were drawn from the same population.

The distinction looks even less clear-cut at $z \simeq 0.3$–0.4, where the spectra of both red and blue galaxies are qualitatively very similar (Fig. 7). After correcting for the effect of Malmquist bias in H-ATLAS, we find that, at a constant stellar mass the space-density of these optically red star-forming galaxies, which are missing from most optical studies, is at least as high as the space-density of the optically blue star-forming galaxies that are included in optical studies. O17 reached a similar conclusion from their reanalysis of the optically selected SDSS galaxy sample.

The combination of the second and third results points to a very different picture of the galaxy population than the standard division into two dichotomous classes – whether one calls these classes 'late-type' and 'early-type', 'star-forming' and 'passive', 'star-forming' and 'red-and-dead', or 'star-forming' and 'quenched'. The smooth appearance of the GS when all galaxies are plotted rather than just galaxies classified as 'star-forming' (Figs 1 and 3), the gradual change in galaxy morphology along the GS (Fig. 1), the fact that the average galaxy spectra change gradually along the GS (Figs 6 and 7), the strong evolution shown by both optically red and optically blue galaxies – all of these suggest that galaxies are better treated as a unitary population rather than two dichotomous classes. As we discuss in Section 5.5, there is actually a lot of recent evidence from observations in other wavebands that leads to the same conclusion.

If our conclusion is correct that galaxies form a unitary population rather than two dichotomous classes, much of the rationale for rapid quenching models (Section 1) vanishes.

Finally in this section we consider the identity of the galaxies producing the rapid low-redshift evolution. The smoking gun is possibly Fig. 7. The stacked spectra in this figure show that the high-redshift H-ATLAS galaxies both contain an old stellar population, shown by the significant 4000 Å spectral break (and the red optical colours), but are also forming stars at a high rate, shown by the UV emission and strong emission lines. The galaxies used to produce these average spectra all have stellar masses $>10^{10.5}\,\mathrm{M}_{\odot}$. Today most galaxies with stellar masses this high are ETGs (Fig. 1). Therefore it seems likely that the H-ATLAS galaxies are the fairly recent ancestors of some part of the ETG population in the Universe today.

Arguments based on chemical abundances imply that at least 50 per cent of the stellar mass of ETGs formed over $\simeq$8 billion years in the past (Thomas et al. 2005), but our results and those of Bourne et al. (2012) suggest that even looking back a few billion years is enough to see significantly enhanced star-formation rates in the ETG population.

5.2 Comparison with theoretical models

The recent large-area galaxy surveys, H-ATLAS in the far-infrared and GAMA in the optical, have made it possible to observe galaxy evolution, with good time resolution, over the last few billion years. The models have not kept pace with the observations and most theoretical papers make predictions over a longer time period with much coarser time resolution. It is therefore not possible to make a definitive comparison of our new results with the results from numerical galaxy simulations such as Illustris and EAGLE, although we do make a comparison with the predictions in a very recent EAGLE paper at the end of this section. We have therefore mostly used an analytic galaxy-evolution model to try to reproduce our results, which does have the advantage that it is generally easier to diagnose why an analytic model does not match the results than is the case for a numerical model.

Given the clear evidence that the increased star-formation rate in galaxies at high redshift is because they contain more gas, both evidence from our results (Dunne et al. 2011) and from those of others (Genzel et al. 2015; Scoville et al. 2016), it is reasonable to assume that, to first order, galaxy evolution is governed by the supply of gas. A useful model based on this assumption, which we will use in this section, is the 'bathtub model' or 'gas regulator model' (Bouché et al. 2010; Lilly et al. 2013; Peng & Maiolino 2014). We will use the analytic version of the bathtub model described by Peng & Maiolino (2014; henceforth PM).

The PM model is based on three assumptions: (a) the star formation rate is proportional to the mass of gas in the galaxy; (b) the rate at which gas is flowing out of the galaxy is proportional to the star-formation rate; (c) the rate at which gas is flowing into the galaxy is proportional to the growth rate of the dark-matter halo in which the galaxy is located. The final assumption can be represented by the following equation:

$$\Phi \propto \frac{\mathrm{d}M_{\mathrm{halo}}}{\mathrm{d}t} \tag{11}$$

in which Φ is the gas inflow rate. In their model, PM used the specific mass-increase rate for a halo found in the hydrodynamic simulations of Faucher-Giguère, Keres & Ma (2011):

$$< \frac{1}{M_{\mathrm{halo}}} \frac{\mathrm{d}M_{\mathrm{halo}}}{\mathrm{d}t} > = 0.0336(1+0.91z) \left(\frac{M_{\mathrm{halo}}}{10^{12}\,\mathrm{M}_{\odot}} \right)^{0.06} \times \sqrt{\Omega_M (1+z)^3 + \Omega_{\Lambda}}\ \mathrm{Gyr}^{-1} \tag{12}$$

We will examine whether this model can explain two of the key *Herschel* results. First, let us consider the shape of the GS. In their model, PM show that the equilibrium value of the SSFR of a galaxy is given by:

$$\mathrm{SSFR} = \frac{1}{t - t_{\mathrm{eq}}} \tag{13}$$

in which t_{eq} depends on parameters such as the mass-loading factor for outflows, the fraction of the mass of newly formed stars that is eventually returned to the ISM, and the star-formation efficiency. With the possible exception of the last (Section 4.4), there is no obvious reason why any of these should depend on stellar mass, and so the model predicts that the SSFR should also be independent of stellar mass. Although this is consistent with the relatively flat GMS found in some optical studies (e.g. Peng et al. 2010), it is clearly completely inconsistent with our results and the other recent findings that the GMS is strongly curved (Whitaker et al. 2014; Gavazzi et al. 2015; Lee et al. 2015; Schreiber et al. 2016; Tomczak et al. 2016; O17).

Now let us try to reproduce the rapid low-redshift evolution. We will try to reproduce both the evolution in the position of the GS seen in Fig. 2 and the evolution in the mass of the ISM in galaxies found by Dunne et al. (2011).

Although the two highest redshift bins in Fig. 2 are highly incomplete, our completeness analysis (Section 3.2) showed that at $z < 0.2$ H-ATLAS is fairly complete for stellar masses $>10^{10}\,\mathrm{M}_{\odot}$ once a correction has been made for Malmquist bias (Fig. 4). We therefore fitted a second-order polynomial to the data points in the two lowest redshift bins in Fig. 2 for galaxies with masses $>10^{10}\,\mathrm{M}_{\odot}$. We found that the mean value of SSFR increases by a factor of $\simeq$2.7 between the two bins if no correction is made for Malmquist bias and $\simeq$3.0 if a correction is made. We can use equation (13) to predict how rapidly the mean SSFR should change between bins according to the PM model. If we assume that the galaxy formed 12 Gyr ago and that t_{eq} is insignificant, the predicted change in SSFR between

a redshift of 0.05 and 0.15 is only 1.12, much less than the observed evolution.

Now let us consider the change in the mass of the ISM. Dunne et al. (2011) found that by a redshift of $\simeq$0.45 galaxies contain roughly 5 times as much dust (and therefore gas[3]) as in the Universe today. In the PM model, the equilibrium gas mass is proportional to the gas inflow rate. On this assumption and using equations (11) and (12), we calculate that the gas mass should increase by a factor of $\simeq$1.3 over the redshift range 0.05–0.45.

In both cases, the PM model predicts much weaker evolution than we observe. The physical reason for this is the assumption that the gas inflow rate is proportional to the rate of increase of the mass of the surrounding dark-matter halo (equation 11), since the growth in the masses of dark-matter haloes is very slow at low redshift (equation 12). This will be a problem for any model, analytic or otherwise, in which the gas flow into a galaxy is proportional to the growth rate of the surrounding halo.

Although it is not yet possible to make a definitive comparison with the predictions of the numerical galaxy simulations, we will make a first attempt to see whether these might reproduce the rapid low-redshift evolution using the recent predictions for the star-formation rate function (SFRF; the space-density of galaxies as a function of star-formation rate) by the EAGLE team (Katsianis et al. 2017). Katsianis et al. show predictions for the SFRF at two redshifts in the redshift range of interest: $z = 0.1$ and $z = 0.4$. Inspection of their Fig. 2 shows that the SFRF has a similar shape at the two redshifts but is shifted upwards in star-formation rate by a factor of $\simeq$1.55 from the lower to the higher redshift. This is quite similar to the way the submillimetre luminosity function evolves, because while its shape stays roughly the same, it moves gradually to higher luminosity as the redshift increases (Fig. 8 of this paper; Dye et al. 2010; Wang et al. 2016a; Marchetti et al. 2016). We can make a rough comparison of the observations and the model if we make the assumption that the characteristic luminosity of the best-fitting Schechter function (L_*) is proportional to the star-formation rate. Wang et al. (2016a) and Marchetti et al. (2016) find, respectively, that $L*$ at 250 μm increases by a factor of 3.25 and 3.59 over this redshift range. This is much faster than the evolution predicted by the model, although this difference needs to be confirmed by an analysis in which the observed and predicted quantities are more obviously comparable. One possible way of strengthening the evolution in the simulation would be to reduce the strength of the feedback in massive galaxies (Katsianis, private communication).

5.3 A new model – the flakey faucet model

In this section we present a heuristic model that can reproduce the shape of the GS and the rapid low-redshift evolution. It is based on a model proposed by Peng et al. (2010) to explain the stellar mass functions of red and blue galaxies, which we have modified to explain the new observations.

Peng et al. (2010) showed that the difference between the stellar mass functions of the red and blue galaxies can be explained by a simple quenching model. In their model, a galaxy evolves along the GMS with its star-formation rate being proportional to its stellar mass, thus producing a horizontal GMS on a plot of SSFR versus stellar mass, until a catastrophic quenching event occurs; the galaxy then moves rapidly to the 'red and dead' region of the diagram. The difference between the stellar mass functions of red and blue galaxies (e.g. Baldry et al. 2012) can be explained almost exactly if the probability of quenching is also proportional to stellar mass. However, this model does not explain the curved GS and the rapid low-redshift evolution.

The difference between our model and that of Peng et al. is that we assume something milder occurs when the galaxy is quenched. We assume that the quenching simply consists of the gas supply to the galaxy being turned off. We discuss possible physical explanations of this stochastic disruption of the gas supply in Section 5.4. After the gas supply is turned off, we model the evolution of the galaxy over the SSFR-versus-stellar-mass diagram; it is this post-quenching evolution that produces the curved GS and the rapid low-redshift evolution.

Many of the details of the models are the same. We assume that as long as gas is being supplied to a galaxy, its star-formation rate is proportional to its stellar mass. We also assume like Peng et al. that the mean SSFR of the galaxies to which gas is still being supplied decreases with cosmic time. Using a slight modification of equation (1) of Peng et al., the SSFR of an individual galaxy, as long as gas is being supplied to it, is given by:

$$\frac{\mathrm{SFR}}{M_*} = \mathrm{SSFR} = 2.5 \left(\frac{t}{3.5}\right)^{-2.2} \mathrm{Gyr}^{-1} + k \tag{14}$$

The constant k represents the position of a galaxy relative to the mean SSFR at that time. We assume k remains a constant as long as gas is being supplied to the galaxy. We also assume, like Peng et al., that the quenching probability is proportional to the galaxy's stellar mass:

$$\mathrm{prob}_{\mathrm{quenching}} = c \times M_* \tag{15}$$

The constant c is the first of the parameters of our model.

To model the evolution of the galaxy after the gas supply is turned off, we need to know the gas mass at that time, which is given by:

$$M_{\mathrm{gas}} = \mathrm{SFR}/\epsilon \tag{16}$$

where SFR is the star-formation rate and ϵ is the star-formation efficiency, which is the second of the two parameters in our model. With this equation and the following two equations, we can follow a galaxy's evolution over the SSFR-versus-stellar-mass diagram once the galaxy's gas supply has been turned off:

$$\Delta M_* = \mathrm{SFR}\Delta t \tag{17}$$

$$\Delta M_{\mathrm{gas}} = -\mathrm{SFR}\Delta t \tag{18}$$

in which Δt is an interval of cosmic time.

There are some implicit assumptions behind these equations. We are assuming, as we did in Section 4.4, that the star-formation rate is proportional to the gas mass rather than to a different power of the gas mass (there is evidence for both in the literature; Kennicutt & Evans 2012). Also, despite the evidence in this paper (Section 4.4) and elsewhere that the star-formation efficiency falls with decreasing SSFR, for simplicity we assume it is constant.

We created a realization of this model by continuously injecting stochastically galaxies on to the diagram with a stellar mass of 10^8 M$_\odot$ and an SSFR given by equation (14), starting at a redshift of 4.0 and continuing to the present time. In giving a value of k to each galaxy, we assumed that the distribution of k is a Gaussian distribution with a standard deviation of 0.2 in $\log_{10}$(SSFR). Once the galaxy is injected, we follow its motion across the diagram, as long as the gas supply is switched on, using equations (14) and (17). In each time step, we use equation (15) and a random number

[3] We assume that the gas-to-dust ratio does not evolve significantly.

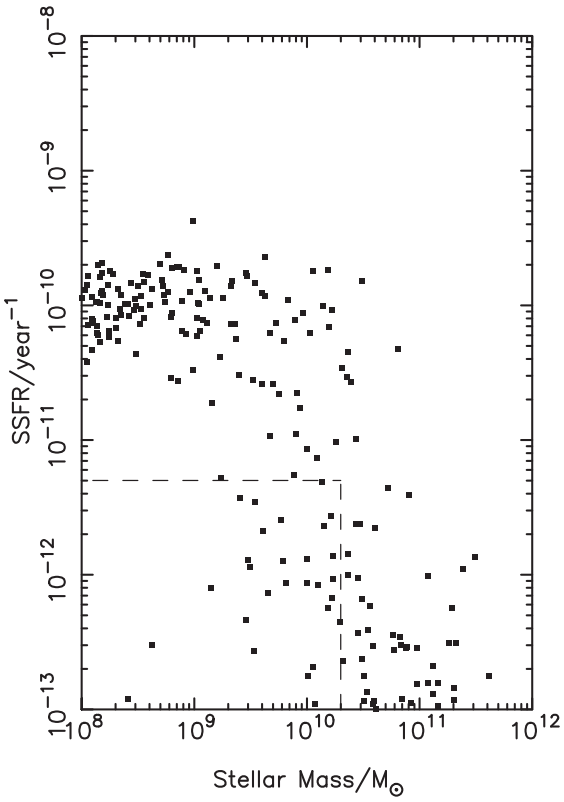

Figure 10. Plot of SSFR against stellar mass at a redshift of 0 for one realization of the flaky faucet model. The figure should be compared with the empirical version of the GS shown in Fig. 1. The galaxies in the box in the bottom left-hand corner would not have been detected in the HRS, and so galaxies in this box do not appear in Fig. 1.

generator to determine whether to switch off the gas supply; once the gas is switched off, we follow the evolution of the galaxy using equations (16)–(18).

We assumed a star-formation efficiency (ϵ in equation 16) of 10^{-9} year^{-1}, a typical value for optically blue galaxies (Section 4.4, Fig. 9). The only other parameter in this model is the quenching probability (c in equation 15), which we adjusted until we got a galaxy distribution in the Universe today that looked like the observed GS. We found that we got reasonable agreement with the observations if

$$\mathrm{prob}_{\mathrm{quenching}}(M_*) = \left(\frac{M_*}{3.3 \times 10^9}\right)\ \mathrm{Gyr}^{-1} \qquad (19)$$

Fig. 10 shows the distribution of the galaxies in a plot of SSFR versus stellar mass at a redshift of 0 for one realization of this model. The dashed lines show the region in the bottom left of the diagram where the HRS is incomplete (Section 2). If one mentally excludes the galaxies in Fig. 10 that fall in this region, the figure's resemblance to Fig. 1, the GS as seen by the HRS, is quite good. The model explains the curvature of the GS as the result of the curved path an individual galaxy follows in this diagram once its gas supply has been cut off. We emphasize that the only thing we have done to get this agreement between the model and the observations is to adjust one parameter: the normalization in the quenching equation (equation 19).

The simplicity of the model means that it is very easy to see what would happen if we change some of its features. In the model, there are no outflows once the gas supply has been turned off. If there continued to be outflows, galaxies would evolve down the diagram more rapidly, reducing the density of points in the figure. On the other hand, if star-formation efficiency decreases with decreasing SSFR, galaxies would move more slowly down the diagram, leading to a greater number of galaxies at intermediate values of SSFR.

Since Fig. 10 shows that most of the galaxies with stellar masses $>10^{10}$ M$_\odot$ in the Universe today are now evolving as closed boxes, the model will naturally lead to strong low-redshift evolution. Dunne et al. (2011) found that by a redshift of $\simeq$0.45, galaxies contain roughly five times more dust (and therefore gas) than today. The simplicity of the model makes a quantitative comparison with the observations pointless, but a rough calculation shows that the model should give approximately the right amount of evolution. If ϵ is the star-formation efficiency, the ratio of the gas mass at time t to the gas mass at $t = 0$ is given by $M_{\mathrm{g}}/M_0 = e^{-\epsilon t}$. An increase of a factor of 5 in the gas mass by $z = 0.45$ requires a star-formation efficiency of $\epsilon = 3.5 \times 10^{-10}$ yr^{-1}. This is close to the centre of the histogram of star-formation efficiencies in Fig. 9. As long as most galaxies are now evolving as closed boxes, the observed evolution in gas mass is easy to explain.

Although this model is outwardly not very different from the model of Peng et al. (2010), its assumptions about the galaxy population are very different. In our model, there is no longer a star-forming GMS and an area of 'red-and-dead' galaxies. Galaxies are still forming stars all the way down the Galaxy Sequence. The only physical distinction is between galaxies which are still being supplied by gas (the horizontal stub of galaxies in Fig. 10) and the galaxies to which the gas supply has been shut off but which are still forming stars.

5.4 Where's the physics?

The heuristic model described in the last section was successful in reproducing in a qualitative and at least in a semiquantitative way some of the key properties of the galaxy population. What physical process could lie behind it? Any process must pass three tests. First, it must be a 'weak quenching' process, stopping any further supply of gas to the galaxy but not removing the gas that is already in the galaxy. Second, it must work in all environments, since the shape of the GS is similar in the field and in clusters (Eales et al. 2017; this paper; O17) and, the rapid low-redshift evolution is also a feature of the overall galaxy population not just the galaxies in clusters.[4] Third, it must have the stochastic element necessary to explain the different stellar mass functions of early- and late-type galaxies.

Many processes suggested as quenching processes fail one or more of these tests. Ram-pressure stripping of gas by an intracluster medium (Gunn & Gott 1972) fails the first and second. Removal of the gas in a galaxy by a wind or jet from an AGN or starburst - 'feedback' – fails the first. Note that we do not claim these processes are not occurring – there is plenty of evidence for feedback, for example (e.g. Cicone et al. 2014) – merely that they are not the process responsible for switching off the gas supply to a galaxy. Galactic 'strangulation' or 'starvation' (Larson, Tinsley & Caldwell 1980), in which the extended gaseous envelope around a galaxy is stripped away, is the kind of weak quenching process we require, since once the envelope is removed there will be no further inflow of gas on to the galaxy, but it was originally suggested as a process that would take place in dense environments, thus failing test 2.

[4] The Butcher–Oemler effect in clusters may have been an early example of this rapid low-redshift evolution (Butcher & Oemler 1978).

In the remainder of this section, we describe one process that potentially passes all three tests, although at least part of this is speculation and we do not claim there are no other possibilities.

The mass in the quenching equation (equation 19) is not a characteristic mass because changing the time unit, from Gyr to years for example, changes its value. However, we can derive a characteristic mass using the natural time-scale for the growth of a galaxy, $SSFR^{-1}$. Rewriting equation (19) as the probability of quenching in this time period rather than per Gyr, the characteristic stellar mass is $\simeq 4 \times 10^8$ $M_\odot$, 3×10^9 $M_\odot$ and 9×10^9 $M_\odot$ at $z = 0$, $z = 1$ and $z = 2$, respectively. These correspond to masses of the surrounding dark-matter haloes of $\simeq 6 \times 10^{10}$ $M_\odot$, 4×10^{11} $M_\odot$ and 8×10^{11} $M_\odot$, respectively (Moster, Naab & White 2013). Ideally, the physical process we require should pass both the three tests above and also explain these characteristic masses.

Our speculative process was inspired by numerical simulations of the way gas cools on to galaxies. These simulations show that gas accretes on to galaxies in two ways: a 'hot mode' in which shocks are set up in the gas, heating it to the virial temperature, from which it slowly cools and is accreted by the galaxy; a 'cold mode' in which gas falls freely on to a galaxy along cold flows (Katz et al. 2003; Keres et al. 2005, Keres et al. 2009; Nelson et al. 2013). The simulations imply the transition halo mass below which gas can be supplied efficiently via cold flows is 10^{11}–$10^{11.5}$ $M_\odot$, fairly similar to the values we require. This process therefore provides a possible explanation of the characteristic mass that we observe, although it is worth noting that (a) the transition from cold mode to hot mode may actually be rather gentle, occurring over a range of halo mass (Nelson et al. 2013), and (b) our attempt to use lensed *Herschel* sources to estimate the mass above which baryons cannot easily accrete on to galaxies gives a value $\simeq$10 times higher than the predictions of the numerical simulations (Amvrosiadis et al. 2017).

The other requirement is stochasticity. Dekel & Birnboim (2006) show that cold flows can still sometimes penetrate to the central galaxy even in haloes above the transition mass. Since the number of cold flows in an individual halo is small, we speculate that whether gas can be still supplied on to a galaxy in a halo above the transition mass may depend on the particular substructure in the individual halo, thus introducing the element of stochasticity that we need.

5.5 Other evidence for a unitary population

There is other recent evidence that instead of two separate classes of galaxies, there is actually a unitary population.

The first evidence comes from the ATLAS^{3D} survey of 260 ETGs. The survey has shown that 86 per cent of ETGs have the velocity field expected for a rotating disc (Emsellem et al. 2011); for 92 per cent of these 'fast rotators' there is also photometric evidence for a stellar disc (Krajnovic et al. 2013). Cappellari et al. (2013) used the ATLAS^{3D} results to propose that there is a gradual change in galaxy properties from LTGs to ETGs rather than a dichotomy at the ETG/LTG boundary. The only exception are the 14 per cent of the ETGs that are 'slow-rotators', for which there is generally (but not always) no photometric evidence for a stellar disc (Krajnovic et al. 2013). Very recently, Cortese et al. (2016), using integral-field spectroscopy from the SAMI survey, have shown that in terms of their kinematic properties LTGs and fast-rotator ETGs form a continuous class of objects.

Other evidence comes from surveys of the ISM in ETGs. The best evidence for the existence of a cool ISM in many ETGs comes from the *Herschel* observations of the ETGs in the *Herschel* Reference Survey. Smith et al. (2012b) detected dust emission from 50 per cent of the HRS ETGs; *Herschel* observations of a much larger sample of ETGs drawn from the ATLAS^{3D} survey have detected a similar percentage (Smith et al. in preparation). The big increase in detection rate from ground-based CO observations of ETGs (e.g. Young et al. 2011) to *Herschel* observations suggests that the common assumption that ETGs do not contain a cool ISM is largely a function of instrumental sensitivity – if we had more sensitive instruments, we would find an even higher fraction with a cool ISM. Interferometric observations of the molecular gas in ETGs generally show a rotating disc similar to what is seen in LTGs (Davis et al. 2013).

Thus these recent results are consistent with our argument that there is a single population of galaxies (with the possible exception of the slow-rotating ETGs – Section 5.6). In our heuristic model (Section 5.3), the dust and gas detected in ETGs are the residual ISM left at the end of their evolution down the GS – these galaxies are ones in which the gas supply was shut off early and have been evolving as closed boxes ever since. A common counter-argument used against this idea is that the kinematics of the gas in ETGs are characteristic of gas acquired as the result of recent mergers. However, the fact that very few ETGs have a gas rotation axis pointing in the opposite direction to the stellar rotation axis, and in the vast majority of the cases the two rotation axes are broadly in the same direction, is strong evidence that most of the gas is this residual ISM (see Eales et al. 2017 for this argument in more detail).

5.6 Steps to a new paradigm

The main argument we have tried to make in this paper and a previous paper (Eales et al. 2017) is that the galaxyscale revealed by *Herschel* does not look much like the predictions of the current paradigm, in which there are two distinct classes of galaxy and a violent quenching process moves a galaxy from one class to the other. The curved Galaxy Sequence shown in Fig. 1, with the gradual change in galaxy morphology along it, seems to us to require a gentler quenching process. The one we have suggested in Section 5.3 is the stochastic removal of the gas supply (a possible physical process is suggested in Section 5.4). If we are correct, the motion of galaxies along the Galaxy Sequence, as well as the rapid low-redshift evolution, is caused, not by the actual removal of the gas supply, but by the gradual evolution that occurs once the gas is turned off.

A number of other groups have also recently investigated quenching processes in the galaxy population. Casado et al. (2015) found evidence for a weak quenching process in low-density environments but for strong quenching in clusters, whereas Schawinski et al. (2014) found evidence for weak quenching in late-type galaxies but strong quenching in early-type galaxies. Peng, Maiolino & Cochrane (2015) used the metallicity distributions of star-forming and passive galaxies to argue that the evolution from one population to the other must have occurred over $\simeq$4 billion years – evidence for weak quenching.

O17 reached a similar conclusion to us about the distribution of galaxies in the plot of SSFR versus stellar mass, but reached a slightly different conclusion about its significance. They concluded that there are actually three types of galaxy: star-forming galaxies, genuinely passive galaxies with no ISM and an intermediate class in which galaxies are still forming stars but with a lower efficiency than in the first class (essentially our optically red class). Our result that the star-formation efficiency declines along the GS (Section 4.4) supports O17's hypothesis of a lower star-formation efficiency in their intermediate class, but the gradual change in morphology along the GS seen in Fig. 1 seems to us evidence against the idea that there

are three physically distinct classes of galaxy. Like us, however, O17 concluded that the evolution from the star-forming class to the intermediate class occurs as the result of the consumption of gas by star formation. Very recently, Bremer et al. (in preparation) have looked at the SEDs and structures of galaxies in the intermediate region of the SSFR-versus-stellar-mass plot, concluding like us that the evolution across this region is the result of the gradual consumption of gas by the formation of stars in the discs of galaxies.

Although there is accumulating evidence for this gentler version of galaxy evolution, there are some unanswered questions.

First, is there a subset of ETGs that are genuinely passive galaxies formed by some violent evolutionary process? One possible class are the 14 per cent of ETGs that are slow rotators (Section 5.5). One way to test this possibility would be to measure the star-formation rate and map the ISM in *all* ETGs, in order to look for the residual star formation and discs that should be present if the only evolutionary process is the weak quenching process we have proposed. Unfortunately, the required observations get extremely challenging for galaxies with $\log_{10}(\mathrm{SSFR}) < -11.5$.

The second bigger question, for which there is also not a definitive answer in the current paradigm, is what causes the morphological variation along the GS seen in Fig. 1? We do not have an answer but a possible clue is that the GS is also a sequence of time: the epoch during which most of the galaxy's stars formed moves earlier as we move down the GS. One idea for forming a galaxy's bulge is that it formed as the result of the rapid motion of star-forming clumps towards the galaxy's centre (Noguchi 1999; Bournaud et al. 2007; Genzel et al. 2011, 2014). We speculate that if this process was more efficient at earlier times, this might explain the morphological change along the GS.

6 SUMMARY

The *Herschel* surveys gave a radically different view of galaxy evolution from optical surveys. We first list our basic observational results.

(i) Rather than a star-forming GMS and a separate region of red-and-dead galaxies, two *Herschel* surveys, selected in completely different ways, reveal a single, curved Galaxy Sequence (GS) extending to low values of specific star-formation rate (Figs 1 and 3). The curvature of the GS confirms other recent results (Whitaker et al. 2014; Gavazzi et al. 2015; Lee et al. 2015; Schreiber et al. 2016; Tomczak et al. 2016; O17) and we show in Section 5.5 that there is plenty of evidence from other wavebands for this picture of a unitary galaxy population rather than two populations.

(ii) The star-formation efficiency (star-formation rate divided by gas mass) falls as one moves down the GS (Section 4.4).

(iii) Galaxy morphology gradually changes as one moves down the GS rather than there being a jump from early-type to late-type galaxies (Fig. 1)

(iv) 15–30 per cent of the galaxies in the far-infrared *Herschel* ATLAS would have been classified as passive galaxies based on their optical colours. We use stacked spectra to show that these red colours are caused by an old stellar population rather than reddening by dust. Nevertheless, these galaxies still contain significant reservoirs of interstellar gas, and the stacked spectra confirm that they are still forming stars. They are red but not dead. After correcting for Malmquist bias, we find that the space-density of optically red star-forming galaxies, which are missed by optical studies, is at least as high as the space-density of optically blue star-forming galaxies of the same stellar mass.

(v) The 250-μm luminosity function of both optically blue and optically red galaxies shows rapid evolution at low redshift, with the evolution appearing stronger for the red galaxies (Section 4.3).

(vi) We use stacked optical spectra of the H-ATLAS galaxies at $0.3 < z < 0.4$ to show that the galaxies responsible for this rapid evolution have a significant spectral break at 4000 Å explaining the red optical colours, but also bright emission lines and a *UV* upturn, implying a high star-formation rate. These galaxies are red but very lively. It seems likely that these galaxies, which have high stellar masses, high star-formation rates and, even a few billion years in the past, an old stellar population, are the relatively recent ancestors of the ETGs in the Universe today.

We have explored whether existing galaxy-evolution models can explain these results. Our conclusion that galaxies are a unitary population lying on a single GS removes the need for a rapid quenching process. We show that the popular gas regulator, or bathtub, model cannot explain the curved GS and the strong low-redshift evolution, and the EAGLE numerical galaxy simulation does not reproduce the strong low-redshift evolution. We propose an alternative model in which the gas supply to galaxies is stochastically cut off (the flaky faucet model). We show that this model provides a natural explanation of the curved GS, while still explaining earlier results such as the difference between the stellar mass functions of optically red and optically blue galaxies. The model naturally explains the rapid low-redshift evolution because most massive galaxies are no longer being supplied by gas and are now evolving as closed boxes.

ACKNOWLEDGEMENTS

We are grateful to the many scientists who have contributed to the success of the *Herschel* ATLAS and the *Herschel* Reference Survey. We thank Antonio Kitsianis for a useful e-mail interchange about his paper on the EAGLE predictions and for supplying a digital version of one of his figures. We also thank an anonymous referee for comments that significantly improved the paper, in particular its readability outside the far-infrared club. EV and SAE acknowledge funding from the UK Science and Technology Facilities Council consolidated grant ST/K000926/1. MS and SAE have received funding from the European Union Seventh Framework Programme ([FP7/2007-2013] [FP7/2007-2011]) under grant agreement No. 607254. PC, LD and SM acknowledge support from the European Research Council (ERC) in the form of Consolidator Grant COSMICDUST (ERC-2014-CoG-647939, PI H L Gomez). SJM LD and RJI acknowledge support from the ERC in the form of the Advanced Investigator Program, COSMICISM (ERC-2012-ADG 20120216, PI R.J. Ivison). GDZ acknowledges financial support from ASI/INAF agreement n.2014-024-R.0.

REFERENCES

Abdo A. et al., 2010, 710, 133
Agius N. et al., 2013, MNRAS, 431, 1929
Amvrosiadis A. et al., 2017, MNRAS, submitted
Baldry I. K. et al., 2012, MNRAS, 441, 2440
Bauer A. et al., 2013, MNRAS, 434, 209
Bell E. F., de Jong R. S., 2001, ApJ, 550, 212
Bell E. F. et al., 2004, ApJ, 608, 752
Bendo G. J. et al., 2010, MNRAS, 402, 1409
Blanton M. R., Roweis S., 2007, AJ, 133, 734
Blanton M. R. et al., 2003, AJ, 125, 2348
Boselli A., Gavazzi G., 2006, PASP, 118, 517
Boselli A. et al., 2010, PASP, 122, 261

Bouché N., Dekel A., Genzel R., 2010, ApJ, 718, 1001
Bournaud F., Elmgreen B. G., Elmgreen D. M., 2007, ApJ, 670, 237
Bourne N. et al., 2012, MNRAS, 421, 3027
Bourne N. et al., 2016, MNRAS, 462, 1714
Bruzual G., Charlot S., 2003, MNRAS, 344, 1000
Butcher H., Oemler A., 1978, ApJ, 219, 18
Cappellari M. et al., 2013, MNRAS, 432, 1862
Casado J., Acasibar Y., Gavilan M., Terlevich R., Terlevich E., Hoyos C., Diaz A. I., 2015, MNRAS, 451, 888
Chabrier G., 2003, PASP, 115, 763
Charlot S., Fall S. M., 2000, ApJ, 539, 718
Cicone C. et al., 2014, A&A, 562, 21
Ciesla L. et al., 2012, A&A, 543, 161
Cortese L. et al., 2012, A&A, 540, 52
Cortese L. et al., 2014, MNRAS, 440, 942
Cortese L. et al., 2016, MNRAS, 463, 170
Da Cunha E., Charlot S., Elbaz D., 2008, MNRAS, 388, 1595
Daddi E. et al., 2007, ApJ, 670, 156
Dariush A. et al., 2011, MNRAS, 418, 64
Dariush A. et al., 2016, MNRAS, 456, 2221
Davies L. J. M. et al., 2016, MNRAS, 461, 458
Davis T. A. et al., 2013, MNRAS, 429, 534
De Vis P. et al., 2017, MNRAS, 464, 4680
Dekel A., Birnboim Y., 2006, MNRAS, 368, 2
Draine B. T. et al., 2007, ApJ, 663, 866
Driver S. et al., 2009, Astron. Geophys., 50, 12
Driver S. et al., 2012, ApJ, 827, 108
Driver S. et al., 2016, MNRAS, 455, 3911
Dunne L. et al., 2011, MNRAS, 417, 1510
Dye S. et al., 2010, AA, 518, L10
Eales S. et al., 2009, ApJ, 707, 1779
Eales S. et al., 2010, PASP, 122, 499
Eales S. et al., 2012, ApJ, 761, 168
Eales S. A. et al., 2015, MNRAS, 452, 3489
Eales S. A. et al., 2017, MNRAS, 465, 3125
Edge A., Sutherland W., Kuijken K., Driver. S., McMahon R., Eales S., Emerson J. P., 2013, The Messenger, 154, 32
Elbaz D. et al., 2007, A&A, 468, 33
Emsellem E. et al., 2011, MNRAS, 414, 888
Faucher-Giguère C. A., Keres D., Ma C.-P., 2011, MNRAS, 417, 2982
Gavazzi G. et al., 2015, A&A, 580, 116
Genzel R. et al., 2011, ApJ, 733, 30
Genzel R. et al., 2014, ApJ, 785, 75
Genzel R. et al., 2015, ApJ, 800, 20
Groves B. et al., 2015, ApJ, 799, 96
Gunn J. E., Gott J. R., 1972, ApJ, 176, 1
Hardcastle M. et al., 2016, MNRAS, 462, 1910
Hayward C., Smith D. J. B., 2015, MNRAS, 446, 1512
Hopkins A. et al., 2013, MNRAS, 430, 2047
Hughes T. M., Cortese L., Boselli A., Gavazzi G., Davies J. I., 2013, A&A, 550, 115
Ilbert O. et al., 2013, A&A, 556, 545
James A., Dunne L., Eales S., Edmunds M., 2002, MNRAS, 335, 753
Katsianis A. et al., 2017, MNRAS, 472, 919
Katz N., Keres D., Davé R., Weinberg D. H., 2003 in Rosenberg J. L., Putman M. E., eds, The IGM/Galaxy Connection. The Distribution of Baryons at $z = 0$, Vol. 281 of Astrophysics and Space Science Library, How Do Galaxies Get Their Gas? p185
Kennicutt R. C., 1998, ARAA, 36, 189
Kennicutt R. C., Evans N. J., 2012, ARAA, 50, 531
Keres N., Hernquist L., 2009, ApJ, 700, L1
Keres D., Katz N., Weinberg D. H., Davé R., 2005, MNRAS, 363, 2
Krajnovic D. et al., 2013, MNRAS, 432, 1768
Larson R. B., Tinsley B. M., Caldwell C. N., 1980, ApJ 237, 692
Lee N. et al., 2015, ApJ, 801, 80
Lilly S. J., Carollo M. C., Pipino A., Renzini A., Peng Y., 2013, ApJ, 772, 119
Liske J. et al., 2015, MNRAS, 452, 2087
Loveday J. et al., 2012, MNRAS, 420, 1239
Marchetti L. et al., 2016, MNRAS, 456, 1999
Martig M., Bournaud F., Teyssier R., Dekel A., 2009, ApJ, 707, 250
Moster B. J., Naab T., White S. D. M., 2013, MNRAS, 428, 3121
Nelson D., Vogelsberger M., Genel S., Sijacki D., Keres D., Springel V., Hernquist L., 2013, MNRAS, 429, 3353
Noeske K. G. et al., 2007, ApJ, 660, L43
Noguchi M., 1999, ApJ, 514, 77
Oemler A., Abramson L. E., Gladders M. D., Dressler A., Poggianti B. M., Vulcani B., 2017, ApJ, 844, 45 (O17)
Page M., Carerra F., 2000, MNRAS, 311, 433
Papadopoulos P., Geach J. E., 2012, ApJ, 757, 157
Peng Y., Maiolino R., Cochrane R., 2015, Nature, 521, 192
Peng Y.-J., Maiolino R., 2014, MNRAS, 443, 3643
Peng Y.-J. et al., 2010, ApJ, 721, 193
Pilbratt G. et al., 2010, A&A, 518, L1
Pineda J. L., Langer W. D., Velusamy T., Goldsmith P. F., 2013, A&A, 554, 103
Planck Collaboration, 2011, A&A, 536, 19
Planck Collaboration, 2014, A&A, 571, 26
Rémy-Ruyer A. et al., 2014, A&A, 563, 31
Renzini A., Peng Y., 2015, ApJ, 801, L29
Rodighiero G. et al., 2011, ApJ, 739, 40
Rowlands K. et al., 2012, MNRAS, 419, 2545
Rowlands K. et al., 2014, MNRAS, 441, 1017
Saintonge A., Tacconi L. J., Fabello S., 2012, ApJ, 758, 73
Sandstrom K. et al., 2013, ApJ, 777, 5
Santini P. et al., 2014, A&A, 562, 30
Schawinski K. et al., 2014, MNRAS, 440, 889
Schreiber C., Elbaz D., Pannella M., Ciesla L., Wang T., Koekemoer A., Rafelski M., Daddi E., 2016, A&A, 589, 35
Scoville N. Z. et al., 2014, ApJ, 783, 84
Scoville N. et al., 2016, ApJ, 820, 83
Smith D. J. B. et al., 2011, MNRAS, 416, 857
Smith D. J. B. et al., 2012a, MNRAS, 427, 703
Smith M. W. L. et al., 2012b, ApJ, 748, 123
Smith M. W. L. et al., 2012c, ApJ, 756, 40
Tacconi L. et al., 2010, Nature, 463, 781
Taylor E. et al., 2011, MNRAS, 418, 1587
Thomas D., Maraston C., Bender R., Mendes de Oliveira C., 2005, ApJ, 621, 673
Tomczak A. et al., 2016, ApJ, 817, 118
Toomre A., 1977, in Tinsley B. M., Larson R. B., eds, Evolution of Galaxies and Stellar Populations, Proceedings of a Conference at Yale University. (Yale University Observatory, New Haven, CT), 401
Tremonti C. et al., 2004, ApJ, 613, 898
Valiante E. et al., 2016, MNRAS, 562, 3146
Wang L. et al., 2016a, A&A, 592, L5
Wang L. et al., 2016b, MNRAS, 461, 1719
Whitaker K., van Dokkum P. G., Brammer G., Franx M., 2012, ApJ, 754, 29
Whitaker K. et al., 2014, ApJ, 795, 104
Young L. M. et al., 2011, MNRAS, 414, 940
Zibetti S., Charlot S., Rix H.-W., 2009, MNRAS, 400, 1181

This paper has been typeset from a TEX/LATEX file prepared by the author.